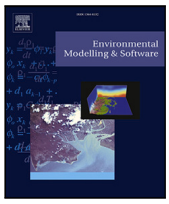
Environmental Modelling and Software 183 (2025) 106214



Contents lists available at ScienceDirect

Environmental Modelling and Software

journal homepage: www.elsevier.com/locate/envsoft



Position Paper

FastFuels: Advancing wildland fire modeling with high-resolution 3D fuel data and data assimilation

Anthony Marcozzi [a,*], Lucas Wells [a], Russell Parsons [b], Eric Mueller [c], Rodman Linn [d], J. Kevin Hiers [e]

[a] New Mexico Consortium, Los Alamos, NM, 87544, USA
[b] USDA Forest Service, Fire Sciences Lab, Missoula, MT, 59808, USA
[c] Fire Research Division, National Institute of Standards and Technology, Gaithersburg, MD, 20899, USA
[d] Los Alamos National Laboratory, Los Alamos, NM, 87545, USA
[e] Texas A&M Natural Resources Institute, Washington D.C., USA

ARTICLE INFO

Dataset link: https://github.com/silvxlabs/fastfuels-core, 10.5281/zenodo.11640691

Keywords:
Fuel modeling
Remote sensing
Wildfire modeling
Wildland fire
Prescribed fire

ABSTRACT

Acquiring detailed 3D fuel data for advanced fire models remains challenging, particularly at large scales. To address this need, we present FastFuels, a novel platform designed to generate detailed 3D fuel data and accelerate the use of advanced fire models. FastFuels integrates existing fuel and spatial data with innovative modeling techniques to represent complex 3D fuel arrangements across landscapes. It leverages data sources including the Forest Inventory and Analysis (FIA) database and plot imputation maps, and incorporates advanced features such as data assimilation from LiDAR. This research demonstrates FastFuels' capabilities through two applications: evaluating fuel treatment effectiveness with the Fire Dynamics Simulator and simulating a prescribed fire operation using QUIC-Fire. FastFuels provides previously unavailable 3D fuel data at landscape scales, empowering informed decision-making, detailed investigations of fuel treatment impacts, and higher-resolution risk assessments. Its flexible data assimilation and model-agnostic outputs accelerate advanced fire science and support fire management decisions.

1. Introduction

Climate change-driven increases in extreme temperatures and drought (Masson-Delmotte et al., 2021) profoundly affect fire regimes, extending fire season length (Flannigan et al., 2000; Halofsky et al., 2020), expanding area burned (Abatzoglou and Williams, 2016; Turco et al., 2018, 2023), and increasing occurrence of extreme events and associated impacts (Lannom et al., 2014). The combined effect of these climate change factors, along with fuel accumulations arising from past management practices (Graham et al., 2004) and increasing intersections between human populations and fire-prone ecosystems (Bowman et al., 2017; Radeloff et al., 2018; Ager et al., 2019), leads to increasing wildfire danger for communities and ecosystems, as well as higher costs associated with fire management and suppression (Doerr and Santín, 2016). Collectively, these factors result in both higher risks, and higher uncertainties for fire and fuel managers.

While the circumstances facing managers are increasingly unprecedented, decades of fire and landscape ecology research authoritatively characterize fire as a natural disturbance process in most ecosystems, playing a key role in maintaining ecosystem function and structure (Graham et al., 2004; Hessburg et al., 2019). Over the last two decades, this understanding has been represented in US land management agency policies, which have sought to shift from a fire suppression focus towards more proactive approaches in fuels management such as fuel treatments and prescribed fire (Stephens et al., 2016). Such practices are critical to restoring ecosystem function and in promoting resilience (Graham et al., 2004; Loudermilk et al., 2017; Hessburg et al., 2019; Halofsky et al., 2020).

However, while policy and science support a more holistic, ecologically-minded consideration of fire management, in practice, fire management continues to primarily focus on fire suppression or exclusion, effectively excluding low-intensity fires from many ecosystems (Kreider et al., 2024; Stephens et al., 2016). A broader range of approaches in responding to wildfires is becoming more common (Young et al., 2020), but the predominant paradigm continues to be fire suppression, often enforced by cultural barriers or societal expectations (Ingalsbee, 2017).

This disconnect between policy intentions and on-the-ground practices is further exacerbated by limitations in the tools available to fire

* Corresponding author.
E-mail address: amarcozzi@newmexicoconsortium.org (A. Marcozzi).

https://doi.org/10.1016/j.envsoft.2024.106214
Received 13 June 2024; Received in revised form 20 August 2024; Accepted 9 September 2024
Available online 18 September 2024
1364-8152/© 2024 Published by Elsevier Ltd.

managers. The decision support systems currently in use, while valuable for immediate operational needs, may not fully capture the complexity required for implementing more nuanced, ecologically-driven management approaches.

At present, the principal operational decision support systems in the United States, such as the Wildland Fire Decision Support System (Noonan-Wright et al., 2011) and the Interagency Fuel Treatment Decision Support System (Drury et al., 2016), use the quasi-empirical Rothermel fire spread model for fire spread simulations (Rothermel, 1972). Though computationally efficient and well suited for operational wildfire support, these models do not account for the full complexity of the physical processes in fire spread and are not sensitive to fine scale variability in fuel structure, composition, or condition—factors which are crucial for accurately predicting fire behavior and effects in both prescribed fire operations and fuel treatment planning (Hiers et al., 2020; Hoffman et al., 2018; Parsons et al., 2018). These shortcomings pose a significant challenge for managers seeking to implement modern, ecologically driven fire management policies and underline the need for new approaches, data and tools.

In recent years, a number of more advanced fire models have emerged which both capture physical fire processes and in which more detailed aspects of fuels have significant impacts on outcomes. These include FIRETEC (Linn et al., 2002), the Fire Dynamics Simulator (FDS)[1] (Mell et al., 2007), both computationally intensive computational fluid dynamics (CFD) fire models, as well as more recent models such as QUIC-Fire (Linn et al., 2020), QES-Fire (Moody et al., 2022), and the level-set formulation of FDS (Bova et al., 2015). These models in general offer a great deal of depth in examining various aspects of fire behavior (Hoffman et al., 2018), and have been applied in numerous studies exploring fire ecology topics, including the impact of bark beetles on fire behavior (Hoffman et al., 2015), fire behavior in spatially discontinuous fuels (Linn et al., 2013), fire behavior and effects in clumpy and patchy fuels (Parsons et al., 2017), as well as impacts of fuel treatments on fire behavior (Parsons et al., 2018; Ziegler et al., 2020). The capacity of such models to explore fuel–fire interactions in disturbed fuels, and to account for how forest structure and composition affect fire behavior, make them highly relevant to ecologically-driven fuel and fire management, where fine scale spatial relationships within the fuel bed can greatly impact both fire behavior and effects (Atchley et al., 2021; Ritter et al., 2023) as well as long term ecosystem function and resilience (Larson and Churchill, 2012; Churchill et al., 2013). However, these models have so far only been used in research and have not been applied operationally, in part due to both their complexity and computational demands.

A critical limiting factor in the use of these models so far has been a lack of detailed 3D fuels data to be used as inputs. Three-dimensional fire models generally require multiple attributes represented in voxels — volumes that contain data, like pixels in an image. While 3D data can be developed from LiDAR or other sources (Marcozzi et al., 2023; Moran et al., 2022; Rocha et al., 2023), the processes required are complex, and in many cases, data may only be available for smaller areas (Moran et al., 2022; Hillman et al., 2021). These limitations have made it difficult to provide 3D fuels inputs for advanced fire models.

In recent years, systems have been developed that facilitate extension of data based on a limited set of observations (such as a fixed-radius plot) to a larger modeled set (such as a forest stand), or to impute key attributes that were not directly measured. These include Fuel Manager (Pimont et al., 2016) and STANDFIRE (Parsons et al., 2018). Both of these systems developed pathways by which forest inventory data in different formats could be translated into 3D fuels inputs for advance fire models. However, neither of these systems provided a means for representing 3D fuels with high detail seamlessly at landscape scales in complex terrain.

[1] https://pages.nist.gov/fds-smv/

Increasingly, modern fire managers must consider the impacts of fuel changes within a stand on fire behavior and fire effects in order to align their management decisions with long term ecological objectives. To meet their needs and to advance the use of physics-based fire models as a critical science tool for wildland fire science, we present here a prototype 3D fuel modeling system, called FastFuels, designed to eliminate or greatly reduce barriers in data availability for advanced fire models. FastFuels links STANDFIRE architecture to forest plot data from the Forest Service's Forest Inventory and Analysis (FIA) program (Gray et al., 2012), leveraging "wall to wall" TreeMap data built on statistical imputation and machine learning (Riley et al., 2021) to provide plot-level 3D fuels data at landscape scales. We describe the system, demonstrate potential applications, and discuss future directions.

2. Methods

2.1. FastFuels overview

FastFuels is a 3D fuel modeling platform designed to accelerate utilization of physics-based wildfire models by providing the detailed, spatially explicit landscape-scale inputs these advanced models require. The system integrates remote sensing imagery and forest inventory plot measurements, combined with statistical and machine learning techniques, to produce comprehensive fuel representations across landscapes in the conterminous United States.

To generate fuels data with wall to wall coverage, FastFuels leverages the US Forest Service's Forest Inventory and Analysis (FIA) Database containing ground measurements of tree attributes from sample plots distributed across the country. Statistical matching and machine learning methods extend these FIA plot data to landscape-level plot imputation maps predicting key fuel parameters. One such example of a plot imputation map is the TreeMap data product. TreeMap uses Random Forest models to impute FIA plots on 30-meter cells across the conterminous United States, producing detailed maps of forest characteristics (Riley et al., 2021). Other approaches, use harmonic regression and clustering to generate plot imputation and attribute maps (Wilson et al., 2018). FastFuels can then reference the FIA database with information from a plot imputation map to populate landscapes with spatially distributed trees representing local stand conditions and distributions.

While FastFuels utilizes default nationwide data sources, it is designed to take advantage of the best available local data for a given area. Local data is essential for characterizing time-dependent changes in forest and landscape conditions. By assimilating diverse data types that observe distinct components of a forest or landscape, FastFuels can develop a more comprehensive perspective of on-the-ground conditions than possible from any single data source alone. For example, aerial LIDAR (ALS) observations can be used to inform individual tree locations, and local plot data can be used to predict tree attributes not present in the ALS data (Roten et al., 2023). The platform integrates these localized inputs with national-scale mapping and data sources to produce customized 3D fuel representations. By synthesizing data across scales, FastFuels generates accurate landscapes reflecting both broad forest patterns and fine-scale stand characteristics, disturbances, and management actions using the best available data for a specific site.

Key FastFuels outputs are delivered in two primary formats: tabular data that catalogs forest inventory, and 2D and 3D grids with spatially explicit biomass attributes that can be converted to input formats for fire behavior models. This flexible data representation enables users to conduct detailed analyses for various tasks including fire behavior modeling, fuel treatment planning, and silvicultural prescriptions. By providing continuous wall-to-wall 3D fuel data at landscape scales, FastFuels helps overcome previous data limitations to enable broader application of advanced physics-based fire models for research, risk management, and operational support. The FastFuels platform adheres to the following guiding design principles:

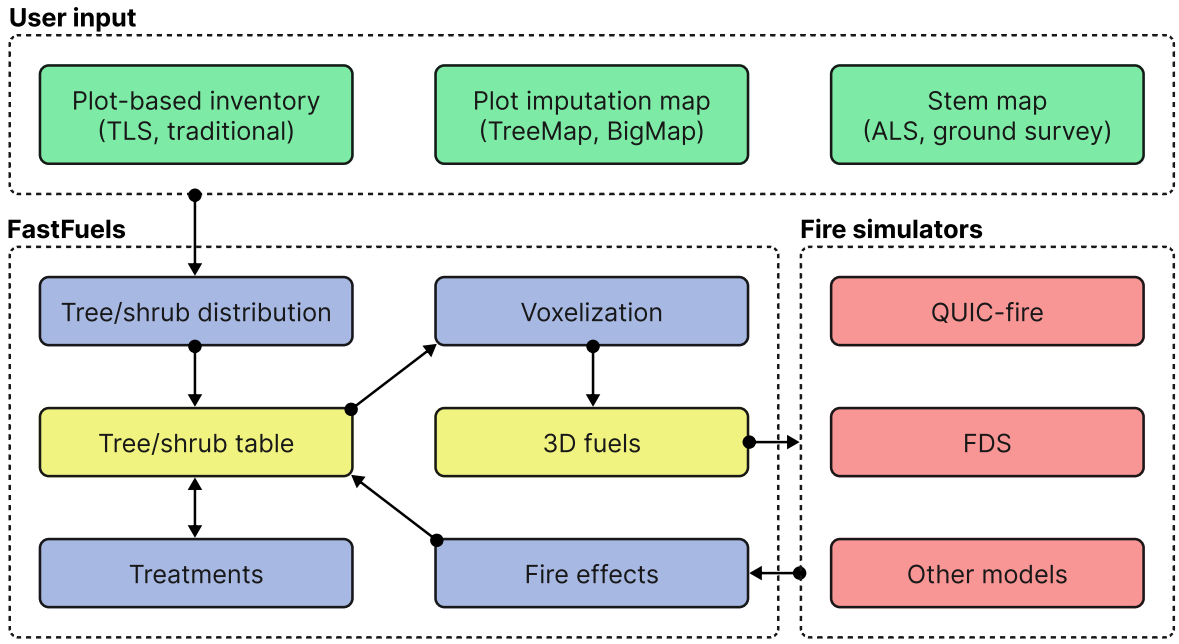


Fig. 1. Overview of the FastFuels modeling pipeline showing the interaction between user inputs, FastFuels, and fire behavior simulations. Green boxes are user inputs, blue boxes are processes internal to FastFuels, yellow boxes are intermediate inputs and outputs, and red boxes are fire simulators.

1. **Scalable architecture**: enabling deployment on platforms ranging from laptops to cloud architectures to high-performance computing centers for easy nationwide data accessibility.
2. **On-demand fuel data generation**: empowering users to rapidly create customized fuel datasets for any area of the contiguous USA.
3. **Flexible data assimilation capabilities**: allowing incorporation of ground and aerial measurements to match on-the-ground conditions.
4. **Mutable data components**: enabling users to simulate treatments, forest growth, fire effects, and natural disturbances.
5. **Model-agnostic storage formats**: facilitating integration with diverse simulation systems and physics-based fire models.

2.2. Input data

FastFuels is a dynamic platform designed to accommodate various types of inventory data, drawing on diverse data sources to generate 3D fuels models. Its adaptability enables it to leverage extensive datasets already available, thus reducing the need for new data collection and expediting the data generation process. The platform is capable of integrating plot-based inventories, plot imputation maps, and stem maps, thereby offering a comprehensive and nuanced input framework (see Fig. 1).

FastFuels can process a wide range of plot-based inventories, including both fixed-radius and variable-radius plot data from small custom sampling protocols to large databases like the Forest Inventory and Analysis (FIA) database (Gray et al., 2012). Plot imputation maps, such as TreeMap from the US Forest Service (Riley et al., 2021), offer a means of large-scale raster data input. TreeMap assigns a best-match plot ID from the FIA database to each grid cell. As such, these maps provide a spatially explicit representation of forest attributes, enabling 3D fuel distributions that closely mirror the actual conditions of specific locations. FastFuels can also process stem maps, including those derived from LiDAR or photogrammetry. These maps provide detailed spatial locations and heights of trees and sometimes include other dendrometric variables. Moreover, FastFuels supports a synergistic use of these diverse data sources. It enables users to integrate multiple sources in a single run, leading to more detailed and nuanced 3D fuels models. For instance, one could use FIA or TreeMap data to extract tree information and supplement it with another plot-based inventory specifically tailored to capture shrubs or other fuel elements.

While FastFuels leverages external data sources to gain extensive coverage of tree data, primarily through forest inventory plots, it is important to recognize the current data limitations for other fuel elements like shrubs or coarse woody debris. Despite this data gap, the principles and methods employed by FastFuels are not limited to trees alone; they are equally applicable to any discrete fuel object. We intentionally define our notation and approach with a focus on trees, given the richness of available data in this domain. However, this framework is flexible and can be adapted to incorporate data on other fuel elements as such information becomes available and integrated into the FastFuels system.

Next, we define the notation representing the input data provided by the user. Let $\mathcal{R} \subset \mathbb{R}^2$ be the region of interest defined by the user as a simple polygon. FastFuels accepts this in various formats, including GeoJSON, Shapefile, and KML. This input geometry is reprojected to Universal Transverse Mercator (UTM) coordinates to minimize distortion in subsequent operations. The axis-aligned bounding box of the input geometry is computed by the function $\Upsilon : \mathbb{R}^2 \to \mathbb{R}^2$ such that $\Upsilon(\mathcal{R})$ produces a rectangle, parallel to the coordinate axes, that contains $\mathcal{R}$. Furthermore, the function $\Phi : \mathbb{R}^2 \to \mathbb{R}$ gives the area of a geometry, such that $\Phi(\mathcal{R})$ is a scalar value for the area of $\mathcal{R}$.

Let $\mathcal{P} \subset \mathbb{N}$ be the index set of forest inventory plots, each with a spatial coordinate $(x_p, y_p) \in \mathcal{R}$. Let $\mathcal{T} \subset \mathbb{N}$ be the index set for measurements taken from trees within the plots. We define a function $\Psi : \mathcal{P} \to 2^{\mathcal{T}}$ that maps each plot $p \in \mathcal{P}$ to a subset of the power set $2^{\mathcal{T}}$, denoted by $\Psi(p)$, representing the trees located in plot p.

Each tree $t \in \mathcal{T}$ is associated with a diameter d_t, a height h_t, a crown ratio r_t, an expansion factor q_t on a per-hectare basis, and a species s_t. Diameter is defined as the diameter at breast height, or the diameter of a tree stem measured at 1.37 m above the ground. Crown ratio is the proportion of total tree length supporting live foliage, and the expansion factor is a factor used to scale each sample tree on a plot to a per-unit area basis. In the case of stem map inputs, we use the notation $(x_t, y_t) \in \mathcal{R}$ to represent the coordinates of each tree. The next section will describe how these coordinates are determined for plot-based tree lists, where the coordinates are not initially known.

2.3. Tree distribution

Plot-based input data sources do not provide explicit spatial coordinates for each tree in the sampled area. Therefore, FastFuels expands the input data to fill the region of interest and assigns spatial coordinates to each tree. This expansion and assignment process is integral to creating a spatially explicit 3D representation of forest fuels, forming the foundation for detailed and realistic 3D fuel distribution from spatially implicit data sources. In the following sections we describe our process for expanding the tree inventory to the region of interest and assigning spatial coordinates to each tree.

2.3.1. Tree list expansion

The initial step in populating the bounding area $Y(\mathcal{R})$ with trees is through a resampling process, guided by tree-level expansion factors. Users have the flexibility to implement this in one of two ways: either by sampling from a combined tree list without considering the specific plot locations, or by using the plot locations to create a Voronoi diagram, and consequently extending the tree list associated with each Voronoi cell.

For the former approach that ignores the plot locations, we begin by determining the number of trees to be resampled, denoted as N. This is calculated using the following equation:

$$N = \mathrm{Poi}\left(\frac{a}{|\mathcal{P}|}\sum_{p\in\mathcal{P}}\sum_{t\in\Psi(p)} q_t\right), \tag{1}$$

where $a = \Phi(Y(\mathcal{R}))$ is the area of the bounding box of $\mathcal{R}$, and q_t represents the per-area basis expansion factor for tree $t \in \Psi(p)$. Here, $\mathrm{Poi}(\lambda)$ denotes a Poisson distribution with mean λ, which is chosen for its property of accurately representing the number of events (in this case, trees) occurring in a fixed interval of time or space.

We define a function $\Gamma : t \to \mathcal{T}'$, where $\mathcal{T}'$ is an indexed set of trees, each of which can appear multiple times with different indices. We use the notation t' to denote the index of each copy of tree t. The resampling process generates a number N of trees to be added to the resampled tree list, and each tree $t \in \mathcal{T}$ is selected with a probability proportional to its expansion factor q_t. This process is repeated N times to generate an indexed resampled tree list $\Gamma(t)$ for each t in $\mathcal{T}$.

In the second approach we use plot locations to create a spatially weighted distribution of tree locations. In this approach we create a Voronoi diagram, denoted as $\mathcal{V}$, using the spatial coordinates of each plot. $\mathcal{V}$ comprises a set of Voronoi cells $\mathcal{V}_p \subset Y(\mathcal{R})$ for each $p \in \mathcal{P}$. Each Voronoi cell $\mathcal{V}_p$ is associated with a specific plot p and represents the region of space closer to its associated plot than to any other plot. The Voronoi diagram is bounded to $Y(\mathcal{R})$.

Rather than resampling trees directly into each Voronoi cell, we consider the bounding box of each Voronoi cell, $Y(\mathcal{V}_p)$. The number of trees to resample in each bounding box, denoted as N_p, is given by the equation:

$$N_p = \mathrm{Poi}\left(a_p \sum_{t\in\Psi(p)} q_t\right), \quad \forall p \in \mathcal{P} \tag{2}$$

where $a_p = \Phi(Y(\mathcal{V}_p))$ represents the area of each bounding box for each Voronoi cell, and q_t is the per-area basis expansion factor for each tree $t \in \Psi(p)$.

In each bounding box $Y(\mathcal{V}_p)$, the resampling procedure generates N_p trees using a bootstrap-like process. Each tree t in the original plot tree list $\Psi(p)$ is selected with a probability proportional to its expansion factor q_t, and this process is repeated N_p times to generate an indexed resampled tree list $\Gamma(t)$ for each t in $\Psi(p)$, populating the bounding box $Y(\mathcal{V}_p)$.

2.3.2. Coordinate assignment

Once the resampled tree list $\Gamma(t)$ has been generated, the next step is to assign spatial coordinates to each tree. The process for assigning these coordinates differs depending on whether plot locations are used.

Without plot locations, we employ a homogeneous Poisson point process, sampling uniformly from the bounding box $Y(\mathcal{R})$, generating a pair of coordinates $(x_t, y_t) \in Y(\mathcal{R})$ for each $t \in \Gamma(t)$. Formally, if $Y(\mathcal{R}) = [x_{\min}, x_{\max}] \times [y_{\min}, y_{\max}]$, then the coordinates are generated as follows:

$$x_{t'} \sim \mathrm{Uni}(x_{\min}, x_{\max}), \ \forall t' \in \Gamma(t), \forall t \in \mathcal{T} \tag{3a}$$

$$y_{t'} \sim \mathrm{Uni}(y_{\min}, y_{\max}), \ \forall t' \in \Gamma(t), \forall t \in \mathcal{T} \tag{3b}$$

where $\mathrm{Uni}(a, b)$ is a uniform distribution on the interval $[a, b]$.

In the presence of plot locations, the process is slightly more complex as it also involves the Voronoi cells. This distribution method is akin to an inhomogeneous Poisson point process as the underlying intensity function varies across space. First, we sample uniformly from the bounding box $Y(V_p)$, yielding an initial set of coordinates C_p for each $p \in \mathcal{P}$. Formally, if $Y(V_p) = [x_{\min,p}, x_{\max,p}] \times [y_{\min,p}, y_{\max,p}]$, the coordinates are generated as follows:

$$x_{t'} \sim \mathrm{Uni}(x_{\min,p}, x_{\max,p}), \ \forall t' \in \Gamma(t), \forall t \in \Psi(p) \tag{4a}$$

$$y_{t'} \sim \mathrm{Uni}(y_{\min,p}, y_{\max,p}), \ \forall t' \in \Gamma(t), \forall t \in \Psi(p) \tag{4b}$$

Next, we refine this initial tree coordinate set C_p by calculating its intersection with the Voronoi cell $\mathcal{V}_p$. This step ensures that each resampled tree lies strictly within the boundaries of the Voronoi cell $\mathcal{V}_p$. This yields the final set of tree coordinates, denoted as C'_p, defined as $C'_p = C_p \cap \mathcal{V}_p$.

For more biologically and ecologically accurate tree distributions, FastFuels offers the option to use advanced point processes. One such option is the Matérn hard-core process, which ensures that trees are not placed too closely to one another by enforcing a minimum distance parameter r between points. This process reflects the natural competition for resources among trees and ensures that trees do not overlap unrealistically. Another option is the Thomas cluster process, which models clustered patterns of trees. In this process, "parent" trees are placed according to a Poisson point process, and around each parent tree, a random number of "offspring" trees are scattered based on a Gaussian distribution. This can be particularly useful for modeling phenomena where trees are naturally clustered, such as in areas with favorable soil conditions or near water sources, or regeneration around seed-bearing adults (see Fig. 2).

2.4. Silvicultural treatments

Forest management treatments are systematic interventions applied to forest stands to achieve specific objectives. These objectives often encompass enhancing forest health, reducing fire risks, improving timber yield, or creating favorable conditions for certain wildlife habitats. The choice of treatment, its intensity, and timing can significantly influence the future trajectory of forest development, resilience to disturbances, and overall ecosystem services provided by the stand.

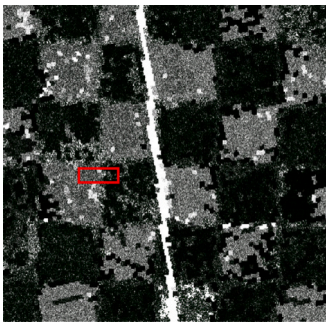
In the context of FastFuels, treatments are used as a means to model potential forest modifications, enabling users to visualize and predict how different interventions might affect forest structure and, subsequently, fire behavior. Implementing these treatments accurately within the FastFuels system ensures that users can make informed decisions about forest management, taking into account both the immediate and long-term implications of their chosen treatment strategies.

2.4.1. Thinning techniques and target conditions

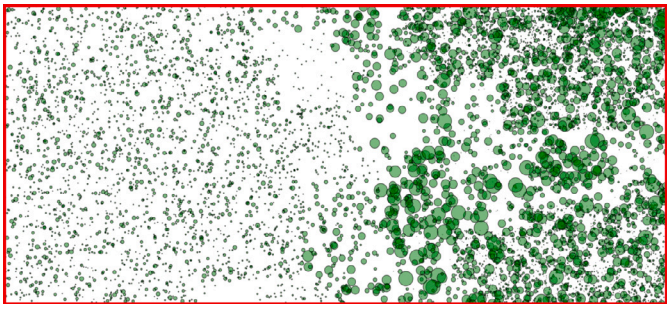
Various thinning techniques can be employed to meet specific stand objectives, ranging from low thinning to crown thinning and proportional thinning. Each of these approaches has unique advantages and implications for forest stand development, and they are often chosen based on the specific goals of the management plan. Below, we delve into each of these thinning methods, detailing their objectives and describing their implementation within the FastFuels framework.



(a) Aerial imagery.



(b) Tree distribution from the TreeMap plot imputation map.



(c) Tree distribution of zoomed area in sub figure b (red rectangle). Circle radii are scaled to crown radius.

Fig. 2. Distribution of trees following an inhomogeneous Poisson point process using a plot imputation map to derive the Voronoi cells.

Low thinning, also referred to as thinning from below, involves the removal of the smallest, often suppressed trees in the lower canopy layer, aiming to reduce the density at the forest floor and enhance the growth of the remaining trees by reducing competition for resources. The main objective is to promote the growth and health of the remaining stand, giving the larger, more dominant trees better access to sunlight, nutrients, and water.

Crown thinning, or thinning from above, primarily targets the dominant and co-dominant trees. Trees are removed from the upper canopy layer, leaving the smaller trees at the lower layers relatively untouched. The goal is to reduce the density of the crown layer, thus improving light penetration and air circulation in the canopy. This promotes the health and vigor of the residual trees by reducing competition in the upper layer of the forest.

Proportional thinning removes trees from all diameter classes in proportion to their representation in the stand. This means that trees of all sizes, from small to large, are removed during the thinning process. The aim is to maintain the same diameter distribution before and after the thinning operation. It strives to ensure that the stand's structural characteristics remain consistent over time.

The choice of thinning technique in forest management is typically guided by specific target conditions, which serve as benchmarks for achieving management objectives. In FastFuels, these conditions can be set using various metrics, each with its own advantages and complexities. We focus here on three commonly used target conditions: basal area (BA); space-based; and individuals, clumps, and openings (ICO).

BA is a simple, non-spatial metric frequently used in the United States to gauge forest stand density. It is particularly accessible for forest managers, with well-established guidelines for target levels, especially for fire risk reduction. An example thin from below to a target basal area of 20 $m^2 \cdot ha^{-1}$ is shown in Fig. 3(a).

Space-based treatments are common in dry, fire-prone areas, particularly in the western United States. The goal is to set a minimum spacing between trees, thereby minimizing the risk of crown fires. Unlike BA targets, this approach requires a level of spatial analysis but remains straightforward in its implementation. An example space-based treatment from below to a target 8 m is shown in Fig. 3(b).

ICO, on the other hand, offers a nuanced approach based on historical reference conditions, aiming to emulate resilient forest structures (Churchill et al., 2013). Though complex to implement, ICO provides a multifaceted, ecologically-based strategy for creating fire-resilient forests. An example thin from below to 6 m ICO clumps is shown in Fig. 3(c).

2.5. Voxelization

Spatially explicit collections of fuel elements, such as trees, are useful data for evaluating landscape characteristics or simulating mechanical thinning. However, many next generation wildland fire models require 3D gridded inputs to represent combustible material in the computational environment. Thus, a key challenge is to convert a spatially explicit description of a tree to a voxelized representation, where a voxel represents a value, or values, on a regular grid in 3D space. To overcome this challenge, we present a nested modeling approach that converts descriptive variables of discrete fuel elements, such as height, diameter, and species, to a 3D grid representation that is appropriate as fuel input to modern coupled fire–atmosphere models such as QUIC-Fire or FDS.

2.5.1. Crown profile models

A variety of mathematical models have been developed to characterize the three-dimensional structure of individual tree crowns. These include probability distribution functions like the beta distribution (Ferrarese et al., 2015) and Weibull distribution (Mori and Hagihara, 1991), geometric shapes like paired paraboloids (Linn et al., 2005), and process-based models that incorporate factors influencing crown morphology such as light availability (Purves et al., 2007). A useful feature common to these crown profile models is that they can be represented geometrically as a solid of revolution. That is, the 3D crown shape can be generated by rotating a 2D profile curve around a central vertical axis aligned with the tree stem. We use this principle to define a function that maps height along the crown axis to radius from the stem, thus encoding the crown geometry for a given model. This provides a generalized method to discretize the irregular crown solid into a regular 3D voxel grid. We present the discretization method using the beta distribution model as an example, but note that the approach can be applied to any of the aforementioned crown profile models.

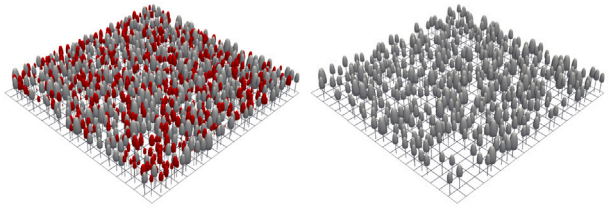
In this work, we utilize a modified beta distribution function to represent species-specific crown shapes following the approach developed in Ferrarese et al. (2015). A beta distribution is a continuous probability distribution defined on the interval $[0, 1]$. The distribution function $\Omega : \mathbb{R} \to \mathbb{R}$ is parameterized by two positive parameters a and b which control the shape of the distribution. The probability density function of the beta distribution is given by:

$$\Omega(\tilde{z}) = \frac{\tilde{z}^{a-1}(1-\tilde{z})^{b-1}}{B(a,b)} \tag{5}$$

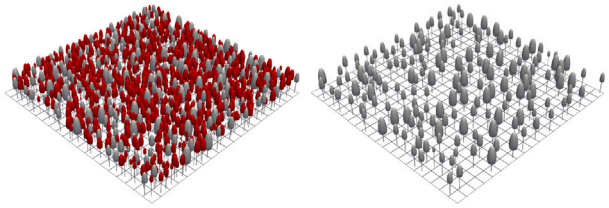
where $B(a, b)$ is the normalization constant to ensure that the total probability is 1, and $\tilde{z} \in [0, 1]$ is an independent variable.

The beta distribution function can be utilized to model tree crown profiles, where the crown shape is described by the interaction between continuous variable $\tilde{z} \in [0, 1]$ and shape parameters a and b. Within this framework, $\tilde{z}$ represents a point along the normalized crown length where $\tilde{z} = 0$ corresponds to the crown base height, signifying the lowest point of the crown, and $\tilde{z} = 1$ denotes the crown height, or the uppermost extremity of the crown. The output $\Omega(\tilde{z})$ expresses the normalized crown radius at a given normalized crown height, $\tilde{z}$.

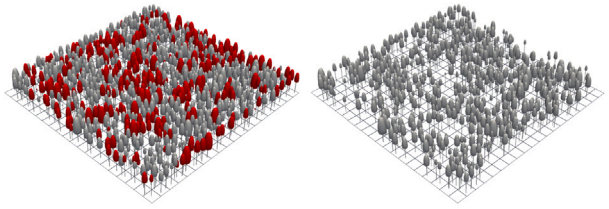
For crown modeling purposes, it is not necessary for the beta probability density function to integrate to 1. Thus, an additional scaling parameter, c, is added to better fit crown profile shapes when $\tilde{z}$ is



(a) Low thinning to 20 $m^2 \cdot ha^{-1}$.



(b) Low thinning to 8 m spacing between stems.



(c) Low thinning to 6 m ICO clumps.

Fig. 3. Examples of tree inventories pre-treatment (left) and post-treatment (right) for three silvicultural prescriptions. Red trees in the pre-treatment sub figures are marked for removal. The pre-treatment stand has 2134 stems per hectare consisting of ponderosa pine (*Pinus ponderosa*) and Douglas-fir (*Pseudotsuga menziesii*) and a basal area of 41.92 $m^2 \cdot ha^{-1}$.

constrained between 0 and 1. With the addition of the scaling term, the modified 3-parameter beta function becomes:

$$\Omega(\tilde{z}) = c\,\frac{\tilde{z}^{a-1}(1-\tilde{z})^{b-1}}{B(a,b)} \tag{6}$$

The actual crown radius in meters at a normalized height $\tilde{z}$ for a given tree $t \in \mathcal{T}$ is then given by:

$$w(\tilde{z}) = h_t r_t \Omega(\tilde{z}) \tag{7}$$

where h_t and r_t represent the height and crown ratio of tree t. Eq. (7) expresses the idea that the normalized crown radius, $\Omega(z)$, is converted to an actual crown radius in meters by multiplying the normalized crown radius by the crown length $h_t r_t$.

Species-specific or species-group specific values for the parameters a, b, and c can be determined by fitting the beta distribution to crown measurements. This approach enables the modeling of various characteristic crown shapes and values, aligning them with observed data.

Crown profiles play an important role in modeling biomass distributions within tree crowns, but are not yet commonly available for all species. To leverage currently available data, FastFuels assigns each tree a set of modified beta distribution parameters by first mapping the tree's FIA species code to one of ten broader species groups (Jenkins et al., 2003). For softwood species, the parameters are assigned based on values from measured canopy profiles of Douglas-fir (*Pseudotsuga menziesii*), Ponderosa pine (*Pinus ponderosa*), and Subapline fir (*Abies lasiocarpa*) in Ferrarese et al. (2015). Douglas-fir parameters are assigned to cedar/larch and Douglas-fir groups, Ponderosa pine parameters are assigned to the Pine group, and Subalpine fir parameters are assigned to the True fir/hemlock and Spruce groups For the remaining hardwood and woodland species groups, the beta parameters were visually estimated to approximate characteristic crown shapes. Going forward, we expect that further research can use a rapidly growing set of TLS data to improve crown profile estimates for additional species, species groups, and other characteristics.

2.5.2. Discretizing a crown profile model to a grid

To generate a voxelized representation of an individual tree $t \in \mathcal{T}$, we first initialize a 3D grid $V \in \mathbb{R}^{n,m,l}$ around the stem location using user-specified grid resolutions $\Delta x, \Delta y, \Delta z$. The number of cells n, m, and l in each dimension are computed based on the tree's maximum crown radius $w(\tilde{z}_{\max})$, height h_t, and crown ratio r_t:

$$n = \left\lceil \frac{w(\tilde{z}_{\max})}{\Delta x} \right\rceil, \quad m = \left\lceil \frac{w(\tilde{z}_{\max})}{\Delta y} \right\rceil, \quad l = \left\lceil \frac{h_t r_t}{\Delta z} \right\rceil \tag{8}$$

where $\tilde{z}_{\max}$ is the dimensionless mode of the beta distribution, which corresponds to the maximum normalized crown radius that maximizes Eq. (6) and is computed as:

$$\tilde{z}_{\max} = \frac{a-1}{a+b-2} \tag{9}$$

Because l is a parameter derived from user provided input, high Δz values can lead to insufficient vertical cells to adequately resolve the crown profile model on the grid. In practice, we sample the vertical cells at a finer resolution than the user-provided input. Specifically, we introduce a vertical sub-grid with spacing $\Delta z'$, where $\Delta z' \leq \Delta z$, and the number of vertical sub-grid cells is computed as:

$$l' = \left\lceil \frac{h_t r_t}{\Delta z'} \right\rceil \tag{10}$$

The increased granularity enabled by this sub-grid resolution facilitates a more accurate intersection between the continuous crown profile model and the discrete voxel grid. We find that a sub-grid vertical resolution of $\Delta z' = 10\,\text{cm}$ leads to a sufficiently resolved discretized crown profile model while balancing computational cost.

Next, for each cell $v_{ijk'} \in V$, where $1 \leq i \leq m, 1 \leq j \leq n, 1 \leq k' \leq l'$, we determine a fractional volume occupancy value proportional to the intersection between the cell geometry and the mathematical crown profile model. To determine the volume of intersection between the crown profile model and grid cells, we apply the marching squares algorithm to horizontal slices of the grid aligned with the stem axis.

Marching squares is a subset of the marching cubes algorithm which is widely used in computer graphics for creating a mesh over an isosurface (Lorensen and Cline, 1987). We reduce the marching cubes algorithm to the 2D marching squares case, which handles a face of a voxel, to create isolines, or contours, over the crown profile. In this publication we further extend the marching squares algorithm to return an intersection area in the specific use-case of discretizing a tree crown, rather than the common use of the algorithm for approximating isolines. A summary of the algorithm is presented below and a visual guide for the intersection between a cell and the crown profile is presented in Fig. 4.

First, we compute the distance from the stem's position, the origin of the crown profile, to the corner of each 2D cell $v_{ijk'}$. The corners of $v_{ijk'}$ are labeled clockwise starting from the top left as A, B, C, and D, as depicted in Fig. 4. Utilizing these distances, we apply a threshold to classify corners inside the crown profile with a value of 1, and those outside with a value of 0. The marching squares algorithm encodes these corner values into a 4-bit index, representing the 16 possible edge combinations that define the cell interaction, which is computed using the bit-wise OR operation as $A^3B^2C^1D^0$. Given the model assumption that the crown profile forms a solid of revolution, it is sufficient to examine just one quadrant of the non-rotational axes. For this study, we focus on the second quadrant of the xy plane, thereby limiting our analysis to 6 out of the 16 possible edge combinations. This specific

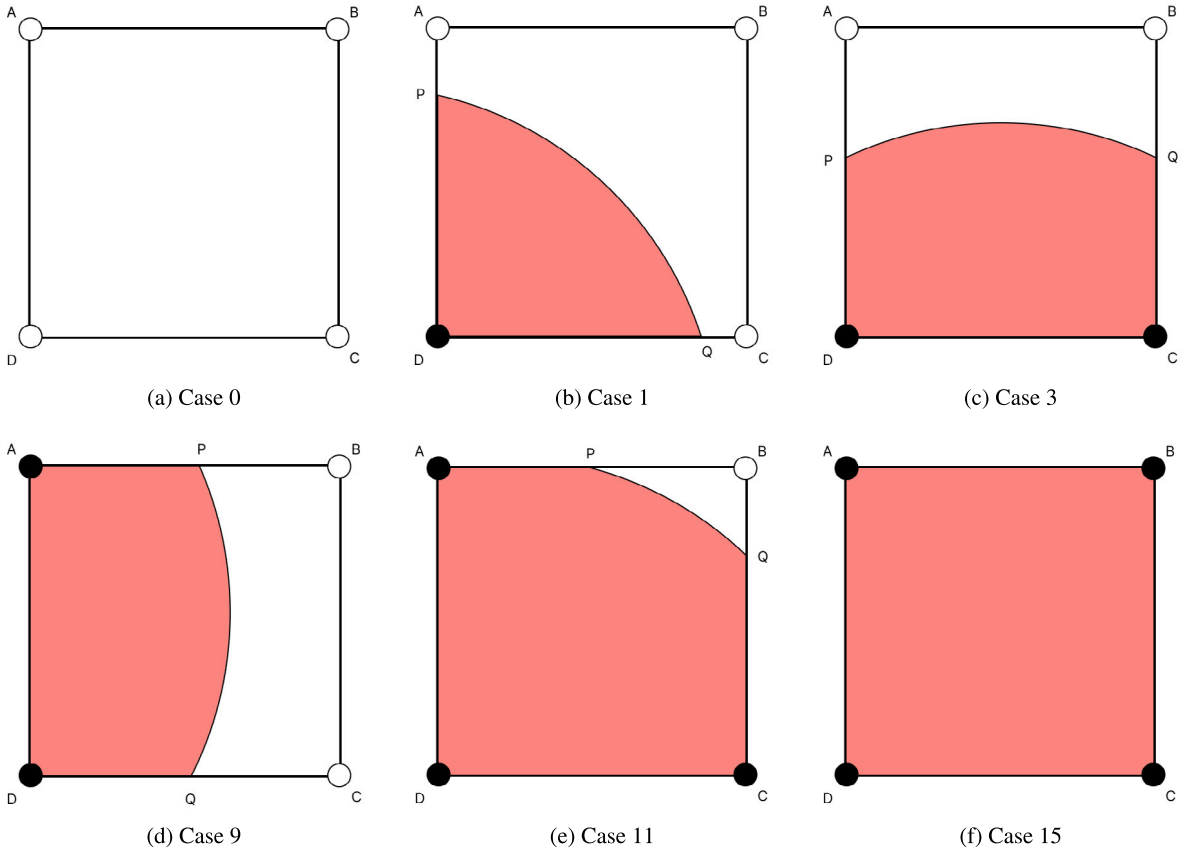


Fig. 4. Marching squares cases showing the different forms of intersection between the crown profile and a grid cell in the second quadrant. The crown profile is a circle centered at point O, which represents the stem position. Corners of the cell, denoted A, B, C, D, are represented by a white circle if they are outside the crown profile and a black circle if they are inside the crown profile. The area of intersection between the cell and the crown profile is shown by the red shaded area. Points P and Q are the points where the crown profile intersects a cell edge.

choice simplifies our model while maintaining its applicability across all four quadrants.

Next, the marching squares algorithm uses a lookup table to populate each cell with contour lines, typically aligning these lines along cell edges through linear interpolation. However, with the crown profile characterized as a circle —its origin and radius explicitly defined, alongside known corner points and a specified case index —we can directly determine the point of intersection between the crown profile and a cell edge. Consider, for instance, a cell exhibiting a Case 1 intersection, as illustrated in Fig. 4(b). Here, the crown profile meets the edge connecting corners $\overline{\mathrm{AD}}$ at point P. The x-coordinate of P, P_x, is known through A_x or D_x, and the unknown y-coordinate P_y is calculated using the circle equation:

$$\mathrm{P}_y = \sqrt{w(\tilde{z}_{k'}) - \mathrm{P}_x^2} \tag{11}$$

where $w(\tilde{z}_{k'})$ is the radius of the crown at the normalized crown length $\tilde{z}_{k'}$ for vertical sub-grid index k', and assuming that the crown is centered at point $(0, 0)$. The same equation is used to find the unknown Q_x coordinate using the known Q_y coordinate and radius. In this way, we find the points P and Q where the crown profile intersects each cell.

Lastly, we use the known case index, the crown profile radius, cell corner points, and the cell-crown profile intersection points to compute the area of intersection between each cell in the slice and the crown profile. Detailed area calculations for each case index are provided in Appendix.

The intersection area approximations computed for each vertical sub-grid layer are summed to obtain the normalized intersection volume between voxel v_{ijk} and the crown model:

$$v_{ijk} = \frac{\sum_{k'=\delta(k-1)+1}^{\delta k} A_{k'} \Delta z'}{\Delta x \Delta y \Delta z} \tag{12}$$

where v_{ijk} is the normalized intersection volume for the voxel will indices i, j, k. $A_{k'}$ represents the intersection area at sub-grid layer k', and $\Delta z'$ is the vertical resolution of the sub-grid layer. The dimensions of the original voxel are denoted by $\Delta x, \Delta y, \Delta z$, and δ is the number of vertical sub-grid cells within each vertical cell in the grid.

A value of $v_{ijk} = 1$ indicates voxel v_{ijk} is completely encapsulated within the crown boundaries. A value of $v_{ijk} = 0$ indicates the voxel is completely outside the crown with no intersection. Fractional values $0 < v_{ijk} < 1$ correspond to voxels partially intersecting the crown model. Fig. 5 shows a vertical slice of volume fraction grid V for an example beta distribution crown profile model discretized to a 3D grid using this approach.

2.5.3. Crown probability grids and occupancy

The next step of the voxelization process is to determine the spatial arrangement of occupied voxels, which represent physical quantities such as biomass, within the discretized crown. Currently, there is a lack of existing research or models that describe the distribution of mass within a crown. To address this gap, we propose a novel modeling technique that aims to capture the characteristics of biomass distribution within a tree crown, based on observable, physiological patterns for biomass allocation and the presence of void spaces. This approach was developed for parameterization with simulated or terrestrial laser scanning (TLS) data, by fitting the parameters to match the observed occupancy patterns. As new research emerges, the model can be updated and refined to incorporate additional terms or alternative approaches that better capture the complexity of crown distributions.

We begin by defining probability grids $P_{xy} \in \mathbb{R}^{n,m,l}$ and $P_z \in \mathbb{R}^{n,m,l}$. These grids represent the probability of the presence of biomass in the horizontal and vertical axis respectively. To define these probability

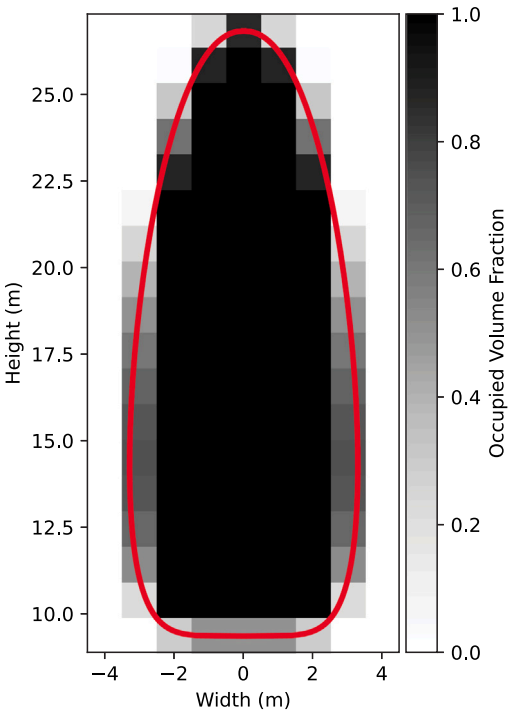


Fig. 5. A 2D cross-section along the center of the x-axis of a ponderosa pine (*Pinus ponderosa*) crown discretized on a 1 m by 1 m by 1 m grid. The grayscale indicates the occupied volume fraction within each grid cell. The beta distribution crown profile model is depicted by the red curve.

distributions, we use two parameters: α and β. The parameter α controls the horizontal, or radial fuel displacement, and the parameter β controls the vertical fuel displacement.

The probability grid P_{xy} represents the probability that a voxel is occupied by biomass as a function of the radial distance from the stem. To compute P_{xy} we first apply distance transform D to each voxel $v \in V$ as:

$$D(v) = \min\{\, \|v - v^*\|_2 \mid v^* \in \mathcal{O} \,\} \tag{13}$$

where $v, v^* \in V$ are voxels in the crown mask, $\|v - v^*\|_2$ is the euclidean distance between voxels v and v^*, and $\mathcal{O} \subset V$ is the set of voxels with a value of 0, or the set of voxels outside of the tree crown. In effect, for each voxel v we apply the transform D to compute the value of the minimum distance from v to some $v^* \in \mathcal{O}$.

Next, the distances in D are inverted as to reflect the maximum distance from the stem, rather than the maximum distance to an edge. The inverted distances D^{-1} are then scaled by the radial distribution term, α:

$$\mathbf{P}_{xy} = \left(D^{-1}\right)^{\alpha} \tag{14}$$

This results in a grid where the probability of a voxel being occupied by biomass is a function of the radial distance from the stem. The exponent α controls the radial probability gradient in $\mathbf{P}_{xy}$. With $\alpha = 0$, the probability is uniform, assigning equal values to all voxels. For positive $\alpha > 0$, probability decays from the crown edge inwards based on the inverse distance. This biases voxel probabilities outward, preferentially increasing the weight of voxels in peripheral crown regions. Negative values of $\alpha < 0$ create the opposite gradient, with probability increasing approaching the stem. This increases the probabilities towards inner crown voxels near the stem. By tuning α, crown fuel profiles ranging from uniform distributions to peripheral or stem-centered patterns can be controlled.

Next, we generate probability grid $\mathbf{P}_z$ to control the probability of occupied voxels along the vertical axis. First, we consider the array $Z \in \mathbb{R}^{n,m,l}$ whose values represent the height above the crown base height, normalized by crown length. We then mathematically transform this height array to create the desired vertical probability distribution using:

$$\mathbf{P}_z = Z^{\beta} \tag{15}$$

where the exponent represents an element-wise exponent on each normalized height in Z.

Raising the voxel heights z to the power of β influences the distribution along the z-axis based on the sign and magnitude of β. When $\beta = 0$, the exponential term has no effect, resulting in a uniform probability distribution with equal values regardless of height. A positive $\beta > 0$ increases probability upwards along the vertical axis, assigning higher probabilities to voxels at greater heights above the crown base. Conversely, negative $\beta < 0$ influences the distribution of probabilities downwards, increasing probability towards voxels lower in the canopy space near the crown base.

After constructing the horizontal probability mask $\mathbf{P}_{xy}$ and vertical probability mask $\mathbf{P}_z$, the next step is combining them to form the joint 3D probability grid $\mathbf{P}_{xyz}$. This is accomplished by multiplying the two masks together element-wise:

$$\mathbf{P}_{xyz} = \mathbf{P}_{xy} \cdot \mathbf{P}_z \tag{16}$$

After normalization, $\mathbf{P}_{xyz}$ contains values in the range $[0, 1]$ representing the joint probability of each voxel being occupied during the biomass distribution process. Voxels with high values in both $\mathbf{P}_{xy}$ and $\mathbf{P}_z$ will have heightened probability in $\mathbf{P}_{xyz}$, while voxels with low values in either mask will have lower probability. This allows sampling voxel occupancy according to the combined radial and vertical probability profiles determined by parameters α and β.

Finally, the last step in determining crown occupancy is a weighted voxel selection process to introduce void space in the tree crown. The amount of void space present in the voxelized tree is quantified through a crown porosity parameter, ρ. Crown porosity is the fraction of empty space within the voxelized canopy and is computed as the ratio of the volume of void space to the total volume of the crown. Voxels are randomly selected without replacement from V and placed in array $M \in \mathbb{R}^{n,m,l}$. The probability of selecting a voxel is weighted by the joint probability P_{xyz}. This process is repeated until M has the desired crown porosity ϕ. The end result of this process is the transformation of a continuous crown shape into a discrete voxel representation with occupied voxels matching the desired crown porosity, and with the spatial distribution of the occupied voxels reflecting the probability gradients in $\mathbf{P}_{xyz}$. Fig. 6 shows the calculation of the probability grids and the selection to a desired crown porosity for an example tree.

We propose this model to offer a parameterizable and representative method that fills the current void in crown structure modeling. This approach, while subject to future refinement, aims to provide a clear and practical foundation for accurately modeling crown structures.

2.5.4. Assigning biomass to occupied cells

Recent coupled fire–atmosphere fire models require gridded, spatially explicit quantities of dry weight biomass, often expressed as mass per volume or bulk density, as model input (Linn et al., 2020; McGrattan et al., 2013). While the occupancy array, M, determines the presence or absence of biomass within a discretized crown, assigning accurate biomass quantities to these occupied voxels requires further modeling. Allometry, the study of the relative growth of different parts of an organism, enables the prediction of dry weight biomass based on readily measured tree attributes such as height, diameter, and species. Numerous allometric models exist at national, regional, and local scales, each with varying degrees of accuracy and applicability depending on specific tree and landscape characteristics (Vorster et al., 2020).

FastFuels offers users the flexibility to select the most appropriate allometric model for their specific scenario, facilitating the integration

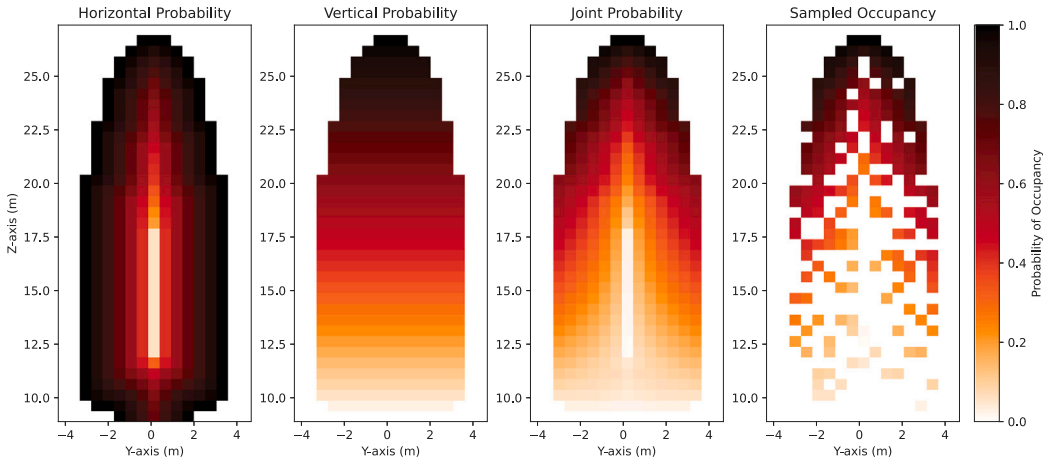


Fig. 6. Horizontal, vertical, and joint probabilities at the central slice of the x-axis for an example ponderosa pine (*Pinus ponderosa*) crown voxelized at 0.5 m by 0.5 m by 0.5 m. The horizontal probability grid is generated with $\alpha = 0.5$ and the vertical probability grid is generated with $\beta = 0.5$. The sampled occupancy grid is sampled without replacement from the joint probability grid to a crown density of $\rho = 0.5$.

of the best available data and knowledge for a given region or species. In addition, the platform is designed to readily incorporate new and improved models as they are developed. For example, the recent FIA National Scale Volume and Biomass estimators (Westfall et al., 2023) can be integrated into FastFuels using a standard modeling approach. To illustrate how FastFuels utilizes allometry for biomass assignment, we present the approach in Jenkins et al. (2003) for predicting dry weight foliage biomass at a national scale. This method, based on a modified meta-analysis of published biomass equations, provides a consistent framework for estimating biomass across diverse species and regions throughout the United States.

To distribute spatially explicit biomass quantities to occupied canopy voxels for tree $t \in \mathcal{T}$, we first estimate the component aboveground biomass as a function of tree diameter and species group as:

$$m_{\text{agb}} = \exp\left(\beta_0 + \beta_1 \ln d_t\right) \tag{17}$$

where m_{agb} is the total dry weight aboveground biomass (kg) for trees with a diameter at breast height greater than 2.5 cm, d_t is the diameter at breast height (cm) for tree t, and β_0 and β_1 are species group specific parameters reported in Jenkins et al. (2003). The aboveground biomass estimate includes biomass from foliage, stem bark, stem wood, and coarse root components. To find component biomass we compute the ratio of component to total aboveground biomass as

$$r_j = \exp\left(\beta_{0,j} + \frac{\beta_{1,j}}{d_t}\right) \tag{18}$$

where the ratio of the biomass of component j to the total above ground biomass is given by $r_j \in [0, 1]$, d_t is the diameter at breast height (cm), and $\beta_{0,j}$ and $\beta_{1,j}$ are component and species group parameters reported in Jenkins et al. (2003). The mass of component j, m_j (kg), is given by the expression:

$$m_j = m_{\text{agb}} r_j \tag{19}$$

Component biomass is then assigned to an occupied voxel according to a distribution mechanism. The most basic mechanism to distribute biomass to occupied voxels is through a uniform method in which each occupied voxel receives an equal quantity of biomass. Other methods may consider the spatial distribution of occupied voxels when distributing biomass, though there is considerable need for future research into these methods. One approach to achieve a spatially heterogeneous approach to distributing biomass without a priori knowledge of distribution mechanisms is to voxelize and uniformly distribute biomass at a fine resolution, then pool voxel biomass quantities to the desired resolution (Marcozzi et al., 2023).

2.5.5. Aligning a voxelized tree to a grid

A voxelized tree, characterized by a collection of voxels denoted as $M \in \mathbb{R}^{n,m,l}$, can be placed within a larger grid that represents a discretized landscape or region of interest. Suppose the bounding box polygon $Y(\mathcal{R})$ is discretized to a three dimensional grid $R \in \mathbb{R}^{n',m',l'}$ where the dimensions n', m', and l' are determined by Eq. (8), corresponding to grid resolutions Δx, Δy, and Δz.

To properly position and orient the tree grid M within the landscape grid R, we assign affine transformation matrices $\tilde{A}_M$ and $\tilde{A}_R$ to the grids. An arbitrary affine transformation on a point set of an affine space, X, can be represented as the composition of a linear transformation and a translation of X. In the finite-dimensional case, an affine transformation of $\mathbb{R}^n$ is a map $F : \mathbb{R}^n \to \mathbb{R}^n$ where the linear map is represented as multiplication by an invertible matrix A, and the translation as addition of the vector $\mathbf{t} \in \mathbb{R}^n$, an affine transform of vector $\mathbf{x} \in \mathbb{R}^n$ can be computed as:

$$\mathbf{y} = F(\mathbf{x}) = A\mathbf{x} + \mathbf{t} \tag{20}$$

Both the linear map and translation can be represented using a single matrix multiplication. In addition, homogeneous coordinates can be used to combine any number of affine transformations into one matrix by multiplying the respective matrices. Vectors are converted to homogeneous coordinates by adding an extra 1, and matrices are converted to homogeneous coordinates by adding an extra row of 0 elements with an extra 1 in the last column. Eq. (20) can be represented as a single matrix multiplication with homogeneous coordinates as:

$$\begin{bmatrix} \mathbf{y} \\ 1 \end{bmatrix} = \left[\begin{array}{ccc|c} & A & & \mathbf{t} \\ 0 & \cdots & 0 & 1 \end{array}\right] \begin{bmatrix} \mathbf{x} \\ 1 \end{bmatrix} \tag{21}$$

where we denote the matrix containing the linear transformation and translation terms as $\tilde{A}$. For a voxelized tree M we construct an affine transformation matrix $\tilde{A}_M$ as:

$$\tilde{A}_M = \begin{bmatrix} \Delta x & 0 & 0 & t_x \\ 0 & -\Delta y & 0 & t_y \\ 0 & 0 & \Delta z & t_z \\ 0 & 0 & 0 & 1 \end{bmatrix} \tag{22}$$

where Δx, Δy, and Δz are scaling terms representing the voxelized tree resolution and the $-\Delta y$ represents the reflective map between the upper left matrix origin and lower left Cartesian origin. In addition, the t_x, t_y, and t_z are translation terms representing the cartesian coordinates of the matrix origin. The affine transformation matrix for the discretized grid $\tilde{A}_R$ is computed in the same manner as Eq. (22).

These constructs are useful because they facilitate the mapping of local matrix coordinates of a voxelized tree to the global matrix coordinates of a voxelized domain. Suppose that $(i, j, k) \in M$ are the matrix

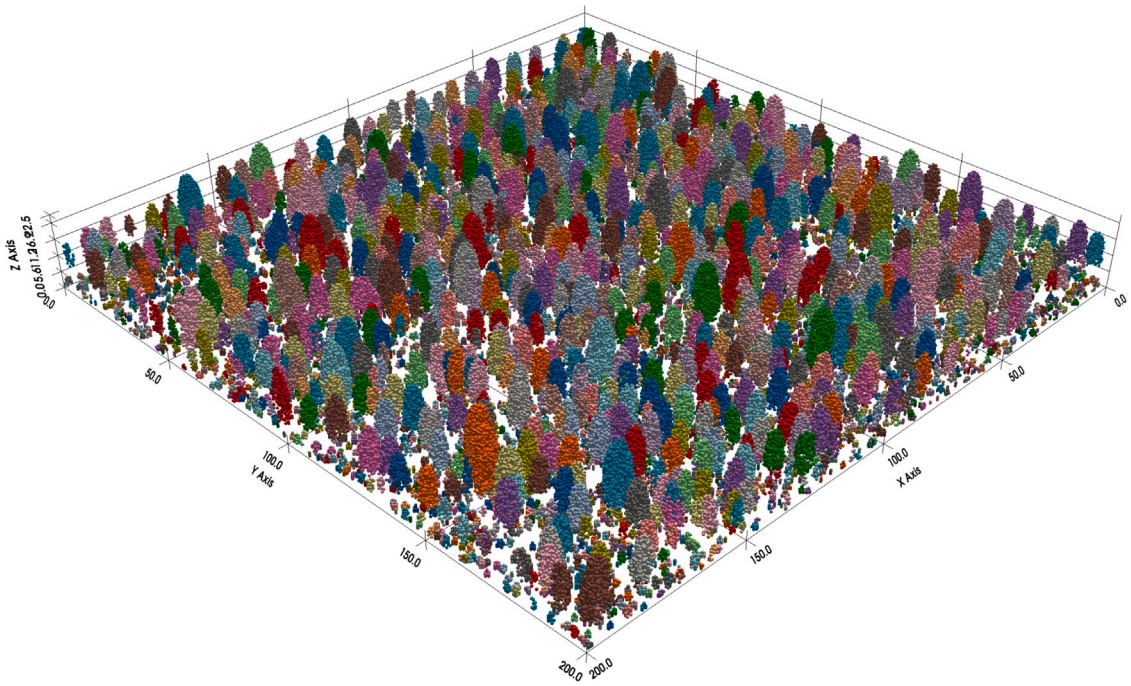


Fig. 7. Voxelized trees placed within a grid representing a forest area spanning 200 m by 200 m by 40 m. The grid's voxel resolution is 0.5 m by 0.5 m by 0.5 m. Distinct colors within the grid indicate individual trees.

coordinates of a voxel containing biomass. Then, the corresponding matrix coordinates $(u, v, w) \in R$ can be computed as:

$$\begin{bmatrix} u & v & w & 1 \end{bmatrix}^T = \tilde{A}_R^{-1} \tilde{A}_M \begin{bmatrix} i & j & k & 1 \end{bmatrix}^T \tag{23}$$

This allows for the merging of the values in M to R as:

$$R_{uvw} = R_{uvw} \odot M_{ijk} \tag{24}$$

where $\odot$ represents an arbitrary operator. In practice, this operator is often the addition operator. For example, if the two grids are merging biomass than the addition operator can be used to combine the additional mass from M_{ijk} with the mass already present in R_{uvw}. However, other operators may be employed. For example, the operator may be a weighted average which takes into account the proportion of biomass already present in a voxel. Fig. 7 shows a collection of voxelized trees that have been placed in a landscape grid using Eq. (24).

In some cases, $\tilde{A}_R$ may not be of the same form as $\tilde{A}_M$. For example, the projection system used to generate the landscape grid R may introduce additional transform terms like rotation or shear that are not present in the voxelized tree grid M. In addition, the tree voxelization algorithm can run at a different grid resolution than the landscape discretization. In these situations, directly merging the voxel values from M to R using Eq. (24) may not give accurate results, as the grid coordinates will not directly align.

Instead, an interpolation procedure like linear interpolation can be used to map the voxel values from M to the appropriately transformed fractional voxel coordinates in R determined by $\tilde{A}_R$. This allows voxelized tree grid M to be accurately integrated into the landscape grid R, handling arbitrary rotation, shear, or resolution differences between the grids.

3. Applications

The capabilities described above illustrate substantial flexibility and power in representing forest fuels as inputs to advanced fire models. In this section we provide two example applications of the FastFuels system to fuel and fire modeling. First, we demonstrate FastFuels as a platform for evaluation of fuel treatments and for analysis of fuel treatment effectiveness. We show how fuels can be manipulated through simulated fuel treatments and demonstrate how these fuel treatments translate to differences in fire behavior and fire effects using the FDS fire model. Then, using a real world management unit in South Carolina, we show the ability of FastFuels to connect with multiple datasets and with the QUIC-Fire fire model to provide predictive capabilities supporting a prescribed fire operation.

3.1. Evaluating fuel treatments with FDS

Frequent, low-intensity surface fires are an important component of historic fire regimes in pine-dominated dry coniferous forests in the western United States. As a result, ponderosa pine (*Pinus ponderosa*) stands were typically maintained in open conditions with large, dominant trees and few shade-tolerant competitors. However, the exclusion of fire from these ecosystems led to altered conditions with many stands dominated by dense thickets of small trees consisting of shade-tolerant species such as Douglas-fir (*Pseudotsuga menziesii*). These changes to ponderosa pine forest structure and composition have led to an elevated risk of stand replacing, extreme wildfires (Arno et al., 1995; Fiedler et al., 2010). As such, there is considerable interest in comparing and contrasting optimal mechanisms for restoring fire resiliency and reducing the risk of extreme fire events in dry forest ecosystems.

In this application, we show that the FastFuels framework is capable of bridging the gap between fuel descriptions and treatments, and measures of fire effects through the use of simulated fire behavior in modern computational fluid dynamics models. This important linkage allows for managers and researchers to make systematic assessments of fuel treatment effectiveness using observed, hypothetical, or remotely sensed data in a modeled environment.

For forest inventory data we selected a plot from the Forest Inventory Analysis program that is representative of a mature ponderosa pine stand with shade-tolerant Douglas-fir encroachment. FIA Plot (PLT_CN) 31453794010690 was measured in October, 2008, and is located in the Blackfoot valley of western Montana.

Two species are present in the plot inventory: Douglas-fir and ponderosa pine. There are 1040 trees per hectare of ponderosa pine with a basal area of 40.14 $m^2 \cdot ha^{-1}$ and a quadratic mean diameter of

22.16 cm. There are 1094 trees per hectare of Douglas-fir and a basal area of 1.78 $m^2 \cdot ha^{-1}$ and a quadratic mean diameter of 4.55 cm.

We first use FastFuels to expand the domain to a 200 m × 200 m area by sampling from a collection of trees without considering plot locations by drawing from the distribution in . Next, we assigned a random location to each tree in the domain. We assigned locations to ponderosa pine with a diameter at breast height greater than 38 cm by applying a Matérn hard-core point process with a radius of 5 m to simulate natural spacing in a mature stand. All other trees were assigned a uniform random location over the domain as expressed in Eq. (3). A visualization of the expanded and distributed plot is shown in the pre-treatment cases in Fig. 3.

In order to examine the effects of mechanical thinning on fire effects we applied two silvicultural treatments to the FIA plot inventory. The silvicultural treatments kept tree locations constant across all cases and had the effect of removing individual trees from the landscape based on the treatment criteria.

First, we simulated a mechanical thinning treatment case which cut trees from below to a desired basal area of 20 $m^2 \cdot ha^{-1}$. This had the effect of removing all of the Douglas-fir, reducing the trees per hectare to 102, and increasing the quadratic mean diameter to 49.85 cm. A visualization of the low treatment plot can be seen in the post-treatment case of Fig. 3(a).

Next, we simulated an individuals, clumps, and openings (ICO) treatment. This treatment case had the effect of removing all Douglas-fir, reducing the trees per hectare to 188, reducing the basal area to 22.38 $m^2 \cdot ha^{-1}$, and increasing the quadratic mean diameter to 38.86 cm. Additionally, this treatment introduced a spatial distribution based on historical reference conditions. A visualization of the ICO treatment plot can be seen in the post-treatment case of Fig. 3(c).

We then used FastFuels to convert a collection of trees to a grid of fuel cells by applying the tree voxelization process described in Section 2.5. Each tree was voxelized to a local grid with dimensions 0.5 m × 0.5 m × 0.5 m using the tree attributes from the FIA Trees table and the species group beta distribution parameters described in 2.5.1. Because the model described in Section 2.5.3 is a conceptual model we currently lack robust parameterization for many species and ecological variations. As such, in order to demonstrate the applicability of the approach to this modeling case we parameterized the algorithm using expert opinion. For the voxelization algorithm we used a radial probability value of $\alpha = 0.5$ and a vertical probability value of $\beta = 0.5$. Crown porosity was set to $\rho = 0$ for crowns with a volume less than 8 m^3, and we applied a linear function to scale crown porosity from $\rho = 0$ to $\rho = 0.75$ for crowns with a volume in the range $[8, 32] m^3$. All crowns with a volume greater than 32 m^3 were given a porosity value of $\rho = 0.75$. Foliage biomass for each tree was computed with Eq. (19) and distributed uniformly to each occupied voxel.

Each local tree grid was then added to a gridded domain representing the 200 m × 200 m area. We gave the domain grid a height of 40 m to accommodate the highest crown height values and each voxel in the grid had a size of 0.5 m × 0.5 m × 0.5 m. Voxels in the local tree grid were merged into the domain grid using Eq. (24). For canopy bulk density we merged the grids using the addition operator, and for fuel moisture content we applied a mean operator weighted by canopy bulk density. A visualization of the voxelized domain for the pre-treatment control case can be seen in Fig. 7 with colors indicating individual trees.

Surface fuels play a critical role in driving fire behavior in dry western forests. Historically, frequent, low-intensity surface fires were sustained by accumulations of surface fuels, primarily consisting of pine needle litter. The spatial heterogeneity of surface fuel bulk density is largely determined by the structure of the forest canopy and prevailing wind conditions. However, accurately capturing the complex dynamics of surface fuel distribution and heterogeneity remains a challenge. New models that take an elliptical transport (McDanold et al., 2023) or a convolutional approach (Sánchez-López et al., 2023) offer promising tools for simulating litter transport and accumulation as a function of overstory distribution, though they require detailed data on litterfall rates and decomposition processes that may not yet be readily available for all scenarios or forest types.

Therefore, in this application, we adopt a simplistic approach, modeling surface fuels as a uniform layer of Long-needle forest floor litter, drawing upon the characteristics of Anderson Fire Behavior Fuel Model 9 (Anderson, 1982). This model fire behavior fuel model, designed for modeling fire spread in closed stands of long-needled pines, like ponderosa pine, specifies a fuel loading of 0.717 $kg\,m^{-2}$ and a fuel bed depth of 6.1 cm. While this simplified approach does not capture the full complexity of surface fuel heterogeneity (Vakili et al., 2016), it provides a reasonable approximation for this demonstration, allowing us to explore the impacts of different canopy fuel treatments on fire behavior and fire effects in a computationally efficient manner.

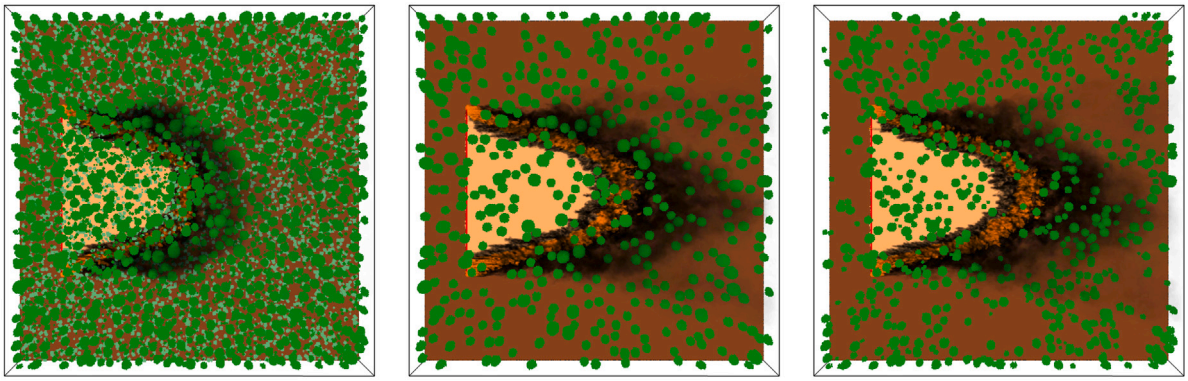
Fuel inputs in the form of bulk density, fuel moisture content, and surface area to volume ratio were provided to the Fire Dynamics Simulator (FDS) model for both the canopy and surface fuel components, using new fuels input capabilities which are being developed as a part of this effort. We assumed that fuel moisture content is uniform across canopy and surface fuel cells and we assigned a fuel moisture content of 100 % to canopy fuels and a fuel moisture content of 15 % to surface fuels. Surface area to volume ratio values were also assigned uniformly with a value of 3422 m^{-1} for Douglas-fire, 3588 m^{-1} for ponderosa pine, 8000 m^{-1} for litter cast surface fuels, and 9770 m^{-1} for grass surface fuels.

Fire Dynamics Simulator (FDS) is a computational fluid dynamics model of fire-driven fluid flow. The model uses a large-eddy simulation model to numerically solve a form of the Navier–Stokes equations appropriate for low-speed, thermally driven flow, with an emphasis on smoke and heat transport from fires on a rectangular grid. FDS uses a particle model to represent objects that cannot be resolved on the numerical grid. In the particle model, different types and quantities of vegetation, like leaves, grass, and needles, are represented by a collection of subgrid particles that are heated via convection and radiation. Fuel inputs were provided to FDS using this particle approach for each occupied canopy and surface voxel.

We ran the FDS model for each fuel arrangement described above in a 200 m × 200 m × 40 m domain. The grid resolution was 25 cm in the horizontal and stretched progressively in the vertical from 12.5 cm at the base up to 2.67 m at the top. To simulate the wind flow through the domain we first ran the FDS model with the untreated fuel arrangement and a uniform wind field. We sampled the adjustment of the velocity field in the canopy along a vertical profile at the downwind edge of the domain. We then specified a characteristic wind speed of 5 $m\,s^{-1}$ and adjusted the wind speed by the relative velocity along the vertical profile. An ignition line was set at 25 m from the upwind boundary and was ignited after 30 s from the start of the simulation. The ignition line released 800 kW/m^2 over 12 s and spread laterally from the center of the domain at 0.5 $m\,s^{-1}$. Each simulation was run until a heat flux threshold of 100 kW/m^2 was reached at a point 150 m from the upwind boundary. A visualization of all three cases after 140 s of simulated time is shown in Fig. 8.

Within the simulation we focused our analysis on a 50 m × 50 m region of interest centered in the middle of the domain. We measured the aggregate rate of spread ($m\,s^{-1}$) and heat release rate (kW/m^2) over the region of interest. In addition, we placed simulated sensors at the stem of each tree which measured the flame height (m) and temperature (°C) at 2 Hz. Flame height was calculated as the vertical height of the volumetric heat release rate greater than a threshold value of 55 kW/m^3.

It is important to note that these simulations are intended as a demonstration of a potential use case for coupling FastFuels with FDS, rather than a detailed validation study. As such, we have applied generic values for vegetation material properties and combustion parameters, based on literature and expert judgement. The exhaustive list



(a) Untreated case (b) Thin from below case (c) ICO thin case

Fig. 8. Visualization of each FDS treatment case after 150 s of simulation time in the Smokeview visualization tool. Ponderosa pine canopy fuel particles are uniformly colored dark green, Douglas-fir canopy fuel particles are uniformly colored teal, and surface fuel particles representing pine litter are uniformly colored brown. Volumetric visualizations of fire and smoke are rendered from heat release rate and soot density.

is not provided here, but can be found in the example input files in the supplementary materials.

We found significant differences in the rate of spread through the region of interest among the three treatment cases considered. Rate of spread was considered to be one-dimensional for this analysis and was computed as the length of the region of interest divided by the time for the leading fire edge to traverse that length. In the untreated case, we observed a rate of spread of $0.56\,\mathrm{m\,s^{-1}}$. In the treatment cases, we saw rates of spread of $0.93\,\mathrm{m\,s^{-1}}$ and $1.02\,\mathrm{m\,s^{-1}}$ for the thin from below and ICO thin treatments, respectively. The effect of performing a mechanical thinning treatment, without modifications to the surface fuel layer, nearly doubled the rate of spread in our simulations. This result corroborates evidence from previous studies which find that open canopies with limited understory reduce fine-scale turbulent wind structures that can block forward fire spread (Atchley et al., 2021; Banerjee et al., 2020; Parsons et al., 2018).

These results highlight the complex interplay between fuel availability and the altered wind field due to changes in canopy structure. Higher fuel loads can increase fire intensity, but dense vegetation also acts as a momentum sink (cf. Buccolieri et al. (2018)), reducing wind speed and thus the rate of fire spread. In the untreated case, the higher fuel load results in a higher heat release rate, but the dense canopy and presence of mid and understory fuels induce higher drag, limiting wind penetration and moderating fire spread. Conversely, the reduced vegetation density in the treated cases allows stronger winds to penetrate and drive the fire, leading to faster fire spread despite the reduced fuel availability. This phenomenon, also observed by Banerjee et al. (2020), aligns with the ecological theory presented by Loudermilk et al. (2022), which emphasizes the importance of vegetation structure in influencing fire behavior beyond its role as fuel. The objective in this case is to provide a tool that can help evaluate these tradeoffs between fuel availability and wind dynamics in physics-based fire models using real-world data.

In addition to aggregate summaries of fire behavior over a region, we can also use the high resolution of the modeled system to draw conclusions about spatially explicit fire effects. For this analysis we limited the fire effects calculations to mature ponderosa pines, defined as ponderosa pines with a diameter at breast height greater than 38 cm, within the region of interest. We estimated scorch height from the maximum flame height each mature ponderosa pine tree using the modeling approach and parameterization in Molina et al. (2022). Next, we computed a probability of mortality from scorch height, height, diameter, and species using the modeling approach in the Fire and Fuels Extension to the Forest Vegetation Simulator (Reinhardt and Crookston, 2003).

We again found significant differences across the treatment cases. The average probability of mortality for the untreated case was 53.17% with a standard deviation of 15.07%. The ICO thin case has a similar average probability of mortality at 51.16%, though the standard deviation was lower at 12.37% and there was a significantly lower maximum probability of mortality at 76.84% compared to the maximum value of 91.58% for the untreated case. The thin from below case had the lowest average probability of mortality of 36.69% with a standard deviation of 12.13%. A map of the probability of mortality after the simulated fire disturbance is shown in Fig. 9. These results suggest that the spatial distribution and the size class of trees following a mechanical treatment have a significant impact on prescribed fire outcomes and fire effects. More importantly, the analysis demonstrates the insights which can be gained from the ability of FastFuels to readily generate these 3D fuel data for use in the FDS model.

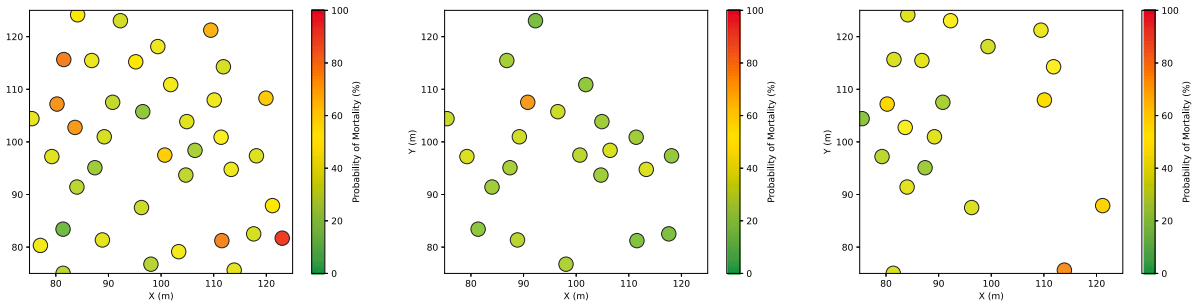
3.2. Simulating prescribed fire with QUIC-fire

The previous application focused on demonstrating our capacity to quantitatively explore how spatially explicit fuel treatments may affect fire behavior and effects. In this application, we demonstrate how FastFuels can offer managers a more detailed and integrative view of prescribed fire as a critical management approach.

The Nature Conservancy's Sandy Island Preserve is located in Georgetown County, South Carolina, and consists of approximately 9165 acres of longleaf pine (*Pinus palustris*) and tidal marsh habitat. In addition, Sandy Island is home to active clusters of endangered red-cockaded woodpeckers (*Leuconotopicus borealis*) that utilize the mature longleaf pine stands. To maintain this fire-dependent ecosystem, prescribed fire is applied frequently across the preserve.

One such area where prescribed fire is frequently applied is the $3.5\,\mathrm{km^2}$ Brookgreen unit in the central region of the Sandy Island Preserve (Fig. 10(a)), characterized primarily by longleaf pine sandhills interspersed with depressional wetlands. The sandy ridges are dominated by mature longleaf pine with a turkey oak understory (*Quercus cerris*), while the depressional wetlands contain dense shrubby vegetation with pocosin fuels.

Prescribed fire objectives for the Brookgreen unit include reducing hazardous fuels, preparing sites for natural longleaf pine regeneration, and controlling encroaching hardwoods like turkey oak. Fire managers must also take special precautions to avoid damaging the high-value mature longleaf pines that provide critical habitat for the endangered woodpeckers. Thus, metrics such as crown scorch are important considerations for evaluation of prescribed fire efficacy. To quantify these burn objectives, the desired outcomes of the prescribed fire include burning 60%–100% of the unit, topkill 20%–50% of the hardwood species, and limiting longleaf pine crown scorch to less than 25%. These



(a) Untreated case (b) Thin from below case (c) ICO thin case

Fig. 9. Spatially explicit fire effects for each treatment case represented in an FDS simulation. Each circle represents a mature ponderosa pine colored by the probability of mortality after exposure to a simulated fire disturbance.

specifications are in addition to important considerations including firefighter and public safety, structures and values at risk, and escapement potential.

Prescribed fire operations for large, heterogeneous landscapes like the Brookgreen unit have historically relied on experienced fire managers using professional judgement to balance complex objectives. However, as prescribed burns become larger and more ambitious, and are applied more broadly at landscape scales, traditional experience-based planning approaches can be limited in their ability to fully evaluate multifaceted goals across diverse terrain, weather conditions, and fuel types. As such, there is a compelling need for new tools to overcome these challenges (Hiers et al., 2020).

Physics-based wildland fire modeling provides advanced capabilities to simulate dynamic fire behavior and effects over space and time. When paired with high-fidelity 3D fuel representations, these models allow for quantitative assessment of fire outcomes in response to changes in fuels, weather, or operational parameters. This systems modeling approach can augment traditional prescribed fire planning by enabling virtual experiments to systematically compare various ignition patterns, fuel conditions, and firing techniques. The FastFuels framework can provide realistic, flexible fuel representations needed to realize the full potential of physics-based wildland fire models like QUIC-Fire for planning and evaluating complex prescribed fires.

To construct a comprehensive 3D fuel representation and simulation inputs for the Brookgreen prescribed fire unit, this work assimilates diverse data sources using the flexible architecture of FastFuels. Tree data for the simulation case are derived from the TreeMap plot imputation map. TreeMap provides a best-match plot ID from the FIA database for each 30-meter gridded cell in the contiguous U.S. (Riley et al., 2021). TreeMap raster values were extracted on a 30 m grid for the region encompassing the burn unit in Fig. 10(a). Individual trees were extracted from each FIA plot in the 30 m grid and then expanded to the bounding box of the burn unit using the plot-based heterogeneous Poisson point process in Eq. (2). This results in a site-specific distribution of trees reflecting species, size classes, crown dimensions, and spatial patterns.

Next, each tree was voxelized at a 2 m by 2 m by 1 m resolution and added to a discretized domain of the same resolution representing the extent of the burn unit following the methods described in Section 2.5. All voxelization parameters and methods were kept the same between the two application cases and are described in Section 3.1. Canopy live fuel moisture was assigned a uniform value of 100 % for all occupied voxels. A canopy height model derived from the voxelized canopy fuels is presented in Fig. 10(c).

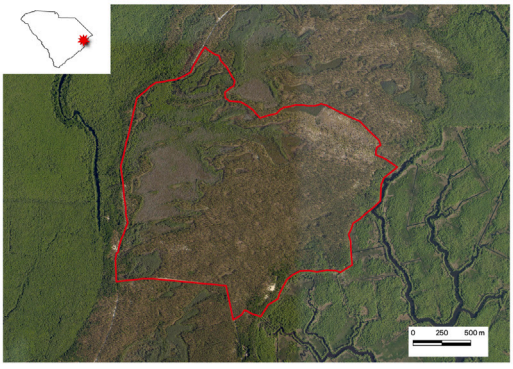
The LANDFIRE 40 Scott and Burgan Fire Behavior Fuel Models (FBFM40) data product provides fire behavior fuel model classification at a 30-meter resolution for the United States (LANDFIRE, 2022). To incorporate surface fuels, the FBFM40 raster was first clipped to the extent of the Brookgreen burn unit polygon. This subset of the fuel model map was converted from discrete categorical values to continuous fuel properties using a lookup table based on the standard fire behavior fuel model parameters published in Scott and Burgan (2005). Fuel characteristics like dead fuel bulk density, fuel bed depth, and extinction moisture content were assigned to each cell based on its classified fuel model type. The fuel characteristics rasters were then resampled from 30 meters to the 2-meter application grid using a cubic spline interpolation method to match the canopy fuel resolution. The resulting rasters of bulk density, fuel bed depth, and fuel moisture content values were supplied to the QUIC-Fire model as the surface fuel inputs. A visualization of the surface bulk density grid is presented in Fig. 10(d).

In this application, we simulated a uniform 20 meter blackline by removing all fuels within 20 meters along the burn unit perimeter. This simplifying assumption allowed us to focus the ignition modeling on the more complex interior strip-heading pattern. The effect of the blackline can be shown in Fig. 10(b) as a black line expanded in the interior of the burn unit in Fig. 10(a), and as an absence of surface bulk density in Fig. 10(d).

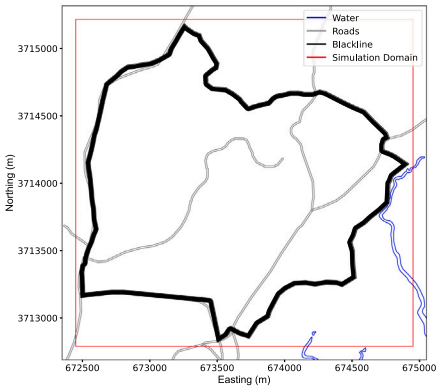
Next, a strip-heading ignition pattern was simulated with four staggered igniters walking at 1.8 m s^{-1} and spaced 15 m apart. The igniters traversed parallel strips across the unit from the blackline edge. Strips had a depth of 10 m between one another. Each igniter used a 10 m dash ignition technique with a 10 m gap between dashes. Ignition strips were separated by a 60 s delay to account for backing fire growth, refueling, and igniter recuperation. This produced an expanding strip-heading pattern emulating operational hand firing techniques which served as time and space dependent ignition input to the QUIC-Fire model. This temporally and spatially explicit modeling approach for simulating realistic ignition patterns will be described and demonstrated in a subsequent publication.

OpenStreetMap (OSM) is an open geospatial database containing vector data on features like roads, water bodies, and other infrastructure (OpenStreetMap contributors, 2017). For this application, road and water polygon layers were extracted from OSM for the extent of the Brookgreen burn unit. These feature layers were rasterized to align with the 2-meter simulation grid cells as shown in Fig. 10(b). The road and water rasters were then used to mask out fuel in areas corresponding to those non-burnable features. Removing fuels from cells overlapping roads and water bodies in OSM creates more realistic fuel grids by explicitly representing barriers to fire spread. Incorporating real-world map data to carve out fuels along roads, rivers, and other mapped features enables more accurate prescribed fire modeling tailored to the on-the-ground conditions of a prescribed fire operation. The flexible FastFuels architecture allows integrating disparate data types like OSM to augment the core tree and surface fuel inputs with other relevant geospatial data sources.

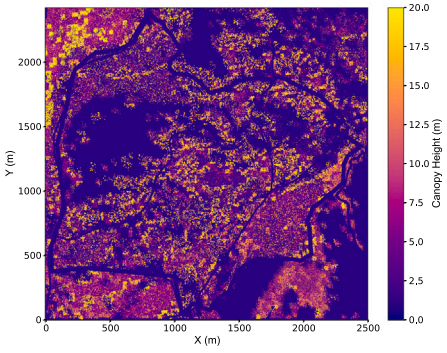
Lastly, we used FastFuels to automatically align the data listed above onto common 2 m by 2 m by 1 m grids and converted them to input files for the QUIC-Fire model. QUIC-Fire is a physics-based wildland fire model that simulates the dynamic interactions between fire, fuels, and atmospheric effects. It couples a fast computational fluid



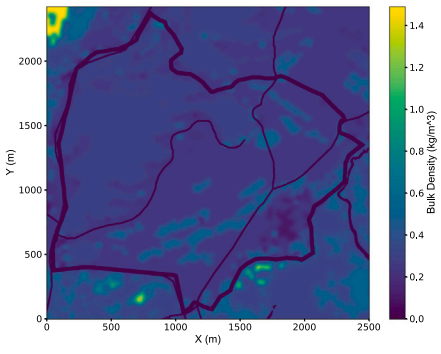
(a) Location of Sandy Island Preserve in South Carolina with an aerial view of the Brookgreen Unit. The unit's boundary is indicated by the red polygon.



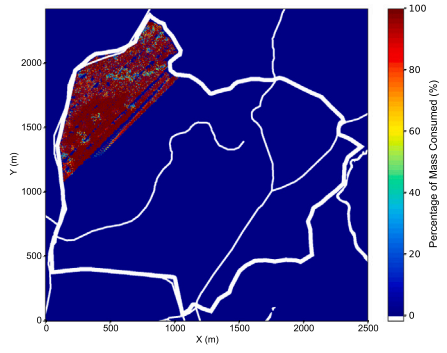
(b) Feature polygons within the Brookgreen Unit that influence fuel distributions, ignition patterns, and fire behavior.



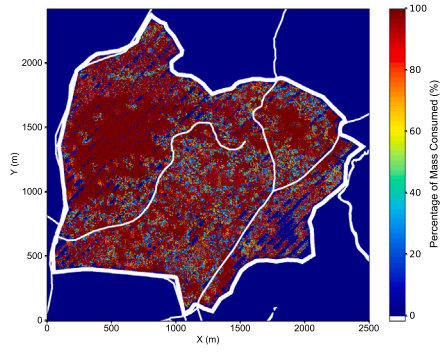
(c) Canopy height model derived from the voxelized canopy. The value of each pixel corresponds to the maximum height above ground.



(d) Surface fuel bulk density distribution in the simulation domain.



(e) Progression of the prescribed fire in the Brookgreen Unit at 6,000 seconds, displaying the vertically integrated percentage of fuel mass consumed.



(f) Progression of the prescribed fire in the Brookgreen Unit at 31,800 seconds, displaying the vertically integrated percentage of fuel mass consumed.

Fig. 10. Integration of diverse data sources to represent and simulate a prescribed fire in the Brookgreen Unit of Sandy Island Preserve. The series of visualizations demonstrate: (a) the geographical context of the preserve and detailed aerial view of the burn unit, (b) influential geospatial features that modify fuel distributions, (c) the canopy height distribution derived from voxelized tree data, (d) surface fuel bulk density distribution, and snapshots of fire progression (e) at 6000 s and (f) at 31,800 s. These visuals underscore the synthesis of high-resolution 3D fuels data, a subset of the geospatial data, and advanced modeling techniques to capture the complexities of a real-world prescribed fire operation.

dynamics wind solver, QUIC-URB, with a cellular automata fire spread model, Fire-CA, to model the two-way feedback between fire behavior and the atmosphere. QUIC-Fire takes spatially explicit 3D data on terrain, vegetation, and ignitions as input. Key outputs include energy release, fuel consumption, particle emissions, wind fields, and other 3D scalar and vector quantities. QUIC-Fire runs faster than traditional CFD fire models which makes it a practical tool for operational prescribed fire planning.

For this application, QUIC-Fire was utilized to simulate the complex prescribed fire ignition pattern and resulting fire progression and effects within the Brookgreen burn unit. The FastFuels framework provided the needed 3D fuel and ignitions inputs. Additional inputs such as a South-easterly wind with a velocity of $1\,\mathrm{m\,s^{-1}}$ measured $2\,\mathrm{m}$ above the ground at the Southwest corner of the burn unit were provided to the model. Topography data for the unit was acquired from the U.S. Geological Survey 3D Elevation Program (3DEP) at $1\,\mathrm{m}$ resolution and was averaged to align with the desired $2\,\mathrm{m}$ simulation resolution. We then ran the QUIC-Fire model for $31\,800\,\mathrm{s}$ of simulated fire behavior and analyzed model outputs to evaluate how well the prescribed fire achieved the management objectives.

The QUIC-Fire simulation demonstrates a successful application of prescribed fire within the Brookgreen unit boundaries to meet the burn objectives. As shown in Figs. 10(e) and 10(f), the fire is confined within the unit perimeter over the duration of the operation, reflecting an appropriate combination of environmental conditions, firing techniques, control lines, and other factors that contribute to operational success in a prescribed fire. By the end of the 31,800 s simulation, a majority of the sub-canopy fuels in the northwest corner of the burn unit were consumed, while there is increasing sparsity in consumption towards the southeast. This could be due to the lower density of canopy fuels in the northwest corner of the unit compared with the ridge along the southwest-northeast axis and the southwest corner.

In this simulation, $87\,\%$ of the surface fuels were consumed in the prescribed fire which meets the original burn objectives of $60\,\%$ to $100\,\%$ consumption. While not considered in this study, simulation outcomes can be compared with additional prescribed fire objectives to further evaluate the effectiveness of the simulated firing operation. For example, scorch height measurements as shown in Section 3.1 or size class and species consumption distributions can be quantified from model output and compared with landscape management objectives.

This single simulation demonstration provides an example realization of prescribed fire on an actual burn unit in the Southeastern United States with important ecological considerations. The input parameters selected here show a successful prescribed fire operation, but small changes in the many factors that affect dynamic fire behavior may have significant impacts on prescribed fire outcomes and public safety. The strength in this modeling approach lies in rapid, accurate data acquisition for a geospatial location, followed by an ensemble modeling technique which runs many iterations of the simulation with small perturbations in the input parameters. By comparing changes in input variables such as wind speed and direction, live and dead fuel moisture content, or firing techniques to changes in output such as rate of spread, area burned, or species consumption, multiple model runs can help inform fire managers of optimal conditions for prescribed fire so as to maximize fire outcomes and firefighter and public safety. The FastFuels system aims to address this critical need in data acquisition to support robust decision making capabilities for prescribed fire.

4. Discussion and conclusions

FastFuels represents a significant advancement in fuel and fire modeling. By providing detailed 3D fuels inputs seamlessly over large areas, FastFuels enables the use of advanced fire models at scales not previously possible. This expands the toolbox for fuel and fire management beyond the current emphasis on 2D, coarse resolution fuel mapping based on rate of spread, and quasi-empirical fire models (Yedinak et al., 2018).

The two application examples presented in this paper demonstrate the potential of FastFuels to support detailed investigations of fuel treatment effectiveness and prescribed fire planning. The ability to represent fuels at tree-level detail, manipulate them with silviculturally realistic treatments, and explore the effects of within-stand spatial fuel arrangements using physics-based fire models within a standardized framework is a major step forward. FastFuels' efficiency, combined with faster 3D fire models like QUIC-Fire, enables ensemble simulations to explore ranges of conditions and treatment intensities, aiding managers in understanding tradeoffs and expanding the solution space for fuel management.

FastFuels addresses previous limitations in data availability by employing novel modeling techniques to represent discrete fuel elements on a landscape as inventory data, and to voxelize fuel elements to 3D grids. Specifically, FastFuels utilizes point processes, such as the Poisson point process and the Matérn hard-core process, to distribute trees realistically across a landscape. This approach accounts for factors like species-specific clustering and competition for resources, resulting in more ecologically accurate fuel representations. Additionally, the platform employs a nested modeling approach to convert individual tree descriptions into 3D voxel models. This involves utilizing crown profile models, probability grids, and biomass distribution mechanisms to capture the complex structure and fuel distribution within tree crowns.

FastFuels also provides a platform for rapidly assimilating new fuels data from a growing array of remote sensing technologies. By developing "onramps" for data from sources like airborne and terrestrial LiDAR and UAS, FastFuels will accelerate the incorporation of new fuel mapping approaches into operational fire modeling. One such approach has been developed to integrate ALS, inventory data, and machine learning approaches to provide improved representations of 3D stand structure (Roten et al., 2023), while other approaches that can take advantage of permutations of remote sensing data products are currently in development.

While FastFuels offers pathways for both new fire models and new fuels data, it has some limitations. Until a broader suite of data assimilation on-ramps are developed, in most cases, the underlying forest inventory data will come from the TreeMap product, which serves as a default datasource. While TreeMap is increasingly used in a range of applications, including providing data for decision support (Calkin et al., 2021), mapping carbon storage and potential loss (Peeler et al., 2023), and classifying old growth (Barnett et al., 2023), it is a relatively new data product that represents the state of the landscape circa 2014 and 2016. Thus, this data thus may not reflect recent disturbances, is constrained to $30\,\mathrm{m}$ classification, and has not yet been subjected to widespread or detailed accuracy assessment (Barnett et al., 2023). Therefore, we expect that errors associated with TreeMap data will propagate to local tree inventory predictions in FastFuels. These issues will likely be mitigated, however, by broader use of the fuel mapping on-ramps as well as future updates to TreeMap. Additionally, new FIA inventory classification methods supported by imagery, large scale field data collection efforts, and machine learning techniques are a high research priority for our team.

Another key limitation of the current FastFuels implementation is that the voxelization model for individual trees lacks robust parameterization across different species, regions, and phenological conditions. The crown probability and occupancy model presented in Section 2.5.3 uses default parameter values that represent a generalized biomass distribution trending outward and upward in the crown. However, these default values may not accurately capture the structural variability present across diverse forest types and ecological contexts. We recognize the need for species-specific and regionally-calibrated parameters to improve model accuracy. To address this limitation, we aim to leverage the growing datasets from terrestrial laser scanning (TLS) efforts to estimate model parameters and perform rigorous validation across

a range of forest conditions (Murphy et al., 2024). By incorporating high-resolution TLS data, we can refine our understanding of crown architecture variability and develop more nuanced parameterizations. This will allow for more accurate representation of biomass distribution within tree crowns, ultimately improving the fidelity of 3D fuel inputs for fire behavior modeling.

Looking ahead, FastFuels can currently be used in conjunction with QUIC-Fire for anywhere in the contiguous United States through two integrative platforms: BurnPro3D[2] and the QUIC-Fire GUI tool. These complementary tools build capacity for project-scale decision support in fuel treatments and prescribed fire planning. In addition, programmatic support for the FDS fire model is currently in development through the qgis2fds plugin[3] for QGIS (QGIS Development Team, 2024). As FastFuels continues to evolve, we envision it as an open-source, model-agnostic platform that welcomes new fuel mapping technologies and provides data for an expanding suite of advanced fire models.

Future research will focus on further refining the platform's capabilities, including the development of additional data assimilation "on-ramps" for emerging remote sensing technologies and improving the parameterization of crown profile and surface fuel models. By fostering cross-disciplinary collaboration and accelerating innovation in fuel mapping and fire modeling, FastFuels aims to provide a powerful tool for advancing wildland fire science and supporting effective fire management in a changing climate.

By connecting state-of-the-art fuels modeling with next-generation fire modeling, FastFuels opens new frontiers for wildland fire science and management in an era of escalating challenges. This advancement holds significant promise for improving wildland fire management strategies and promoting ecosystem resilience.

Funding

This research was funded by the Department of Defense Strategic Environmental Research and Development Program (SERDP) grant numbers RC22-3570 and RC20-1025, as well as Environmental Security Technology Certification Program (ESTCP) grant number RC23-7626.

CRediT authorship contribution statement

Anthony Marcozzi: Writing – review & editing, Writing – original draft, Visualization, Validation, Software, Resources, Methodology, Investigation, Formal analysis, Data curation, Conceptualization. **Lucas Wells:** Writing – review & editing, Writing – original draft, Visualization, Validation, Supervision, Software, Resources, Project administration, Methodology, Investigation, Funding acquisition, Formal analysis, Data curation, Conceptualization. **Russell Parsons:** Writing – review & editing, Writing – original draft, Supervision, Project administration, Funding acquisition, Conceptualization. **Eric Mueller:** Writing – review & editing, Visualization, Validation, Software, Methodology, Formal analysis, Data curation, Conceptualization. **Rodman Linn:** Writing – review & editing, Project administration, Funding acquisition, Conceptualization. **J. Kevin Hiers:** Writing – review & editing, Resources, Project administration, Funding acquisition, Conceptualization.

Declaration of competing interest

The authors declare that they have no known competing financial interests or personal relationships that could have appeared to influence the work reported in this paper.

[2] https://burnpro3d.sdsc.edu/index.html

[3] https://github.com/firetools/qgis2fds

Software and data availability

The algorithms presented in this work are implemented in the Python package **fastfuels-core**, which was authored by Anthony Marcozzi and Lucas Wells in 2024. The package is available for Linux, MacOS, and Windows, and can be freely accessed under the MIT license. The software, written in Python with a program size of 70KB, can be found at https://github.com/silvxlabs/fastfuels-core. The data to reproduce the results of this work are available in a Zenodo repository with DOI 10.5281/zenodo.11640691, and is licensed under the Creative Commons Attribution 4.0 International License. The data archive, sized at 122.9 MB, contains files of gridded fuel inputs, landscape rasters, and fire model outputs used for analysis in this work.

Acknowledgments

The authors thank Matt Snider with the New Mexico Consortium and Devin Yeatman with the Nature Conservancy for their assistance in providing unit descriptions, burn plan objectives, and evaluation for the QUIC-Fire simulation.

Appendix. Intersection geometry

In this section we present the intersection geometry calculations for each of the cases presented in Fig. 4.

A.1. Case 0

This case can be divided into two subcases. In the first case, as seen in Fig. 4(a), none of the cell's corners are inside the crown profile and the area is 0.

It is also possible that the circular crown profile is entirely contained within the cell, but does not contain the cell's corners. In this case, we compute the intersection area as the area of the crown profile, $\text{Area} = \pi w(\tilde{z}_{k'})^2$, for crown radius $w(\tilde{z}_{k'})$ at vertical index k'.

A.2. Case 1

This case occurs when the corner point D is within the boundaries of the crown profile, and can be seen in Fig. 4(b). The intersection area in this case is calculated by summing the areas of two segments. First, we compute the area of the triangle given by $\triangle$ PQD. Next, we compute the "the area of the circular segment defined by chord $\overline{\text{PQ}}$ and the arc given by the crown profile, denoted $\widehat{\text{PQ}}$. The equation used to compute the intersection area for case 1 is as follows:

$$\begin{aligned}
\text{Area} &= \text{Area}_{\triangle\text{PQD}} + \text{Area}_{\widehat{\text{PQ}}} \\
\text{Area}_{\triangle\text{PQD}} &= \frac{1}{2}\left(\text{Q}_x - \text{P}_x\right)\left(\text{P}_y - \text{Q}_y\right) \\
\text{Area}_{\widehat{\text{PQ}}} &= \frac{w(k')^2}{2}\left(\theta - \sin\theta\right) \\
\theta &= 2\arcsin\left(\frac{l}{2w(k')}\right) \\
l &= \|\text{P} - \text{Q}\|_2
\end{aligned} \tag{25}$$

where $w(k')$ is the radius of the crown profile at height k' and l is the length of chord $\overline{\text{PQ}}$.

A.3. Case 3

This case occurs when corner points C and D are within the boundaries of the crown profile, and can be seen in Fig. 4(c). The intersection area in this case is calculated by summing the areas of three segments. First, we compute the area of a triangle formed by points P, Q, and E where E is a point below P, (P_x, Q_y). In scenarios where $\text{P}_y = \text{Q}_y$, then P and E are the same point. In this case, the intersection area of the triangle segment is 0. Secondly, we compute the area of the rectangle

defined by points E, Q, C, and D. Lastly, we compute the area of the circular segment $\widehat{PQ}$. The equation used to compute the intersection area for case 3 is as follows:

$$\begin{aligned} \text{Area} &= \text{Area}_{\triangle PQE} + \text{Area}_{\square EQCD} + \text{Area}_{\widehat{PQ}} \\ \text{Area}_{\triangle PQE} &= \frac{1}{2}\left(Q_x - P_x\right)\left(P_y - Q_y\right) \\ \text{Area}_{\square EQCD} &= \left(Q_y - D_y\right)\left(C_x - D_x\right) \end{aligned} \tag{26}$$

where $\text{Area}_{\widehat{PQ}}$ is given by Eq. (25).

A.4. Case 9

This case occurs when corner points A and B lie within the boundaries of the crown profile, as depicted in Fig. 4(d). Case 9 represents a scenario analogous to Case 3 (described in Appendix A.3), but with a rotational transformation applied. Consequently, the intersection area calculation for Case 9 can be derived by applying the same principles used in Case 3, accounting for the rotation. With E now defined as a point left of Q, (P_x, Q_y), the equation used to compute the intersection area for case 9 is as follows:

$$\begin{aligned} \text{Area} &= \text{Area}_{\triangle PQE} + \text{Area}_{\square APED} + \text{Area}_{\widehat{PQ}} \\ \text{Area}_{\triangle PQE} &= \frac{1}{2}\left(Q_x - P_x\right)\left(P_y - Q_y\right) \\ \text{Area}_{\square APED} &= \left(P_x - A_x\right)\left(P_y - Q_y\right) \end{aligned} \tag{27}$$

where $\text{Area}_{\widehat{PQ}}$ is given by Eq. (25).

A.5. Case 11

This case occurs when corner points A, C, and D are within the boundaries of the crown profile, as depicted in Fig. 4(e). The intersection area in this case is calculated by summing the area of circle segment $\widehat{PQ}$ and the area of the trapezoid defined by the points A, P, Q, C, and D. The area of the trapezoid is computed by subtracting the area of the triangle defined by points P, B, and Q from the area of the cell. The equation used to compute the intersection area for case 3 is as follows:

$$\begin{aligned} \text{Area} &= \text{Area}_{\widehat{PQ}} + \text{Area}_{APQCD} \\ \text{Area}_{APQCD} &= \text{Area}_{\square APED} - \text{Area}_{\triangle PBQ} \\ \text{Area}_{\square APED} &= \left(B_x - A_x\right)\left(A_y - D_y\right) \\ \text{Area}_{\triangle PBQ} &= \frac{1}{2}\left(Q_x - P_x\right)\left(P_y - Q_y\right) \end{aligned} \tag{28}$$

where $\text{Area}_{\widehat{PQ}}$ is given by Eq. (25).

A.6. Case 15

This case occurs when all corner points are within the boundaries of the crown profile, as seen in Fig. 4(f). The intersection area of this case is calculated as the area of the cell.

References

Abatzoglou, J., Williams, A.P., 2016. Impact of anthropogenic climate change on wildfire across Western U.S. forests. Proc. Natl. Acad. Sci. 113 (42), 11770–11775.

Ager, A.A., Palaiologou, P., Evers, C., et al., 2019. Wildfire exposure to the wildland urban interface in the Western U.S.. Appl. Geogr. 111, 102059.

Anderson, H.E., 1982. Aids to determining fuel models for estimating fire behavior. Publication Title: US Department of Agriculture, Forest Service, General Technical Report Issue: INT-22.

Arno, Stephen F., Scott, Joe H., Hartwell, Michael G., 1995. Age-Class Structure of Old Growth Ponderosa Pine/Douglas-fir Stands and Its Relationship to Fire History. U.S. Dept. of Agriculture, Forest Service, Intermountain Research Station, Ogden, UT.

Atchley, A.L., Linn, R., Jonko, A., Hoffman, C., Hyman, J.D., Pimont, F., Sieg, C., Middleton, R.S., 2021. Effects of fuel spatial distribution on wildland fire behaviour. Int. J. Wildland Fire 30 (3), 179–189.

Banerjee, Tirtha, Heilman, Warren, Goodrick, Scott, Hiers, J. Kevin, Linn, Rod, 2020. Effects of canopy midstory management and fuel moisture on wildfire behavior. Sci. Rep. 10 (1), 17312, Number: 1 Publisher: Nature Publishing Group.

Barnett, Kevin, Aplet, Gregory H., Belote, R. Travis, 2023. Classifying, inventorying, and mapping mature and old-growth forests in the United States. Front. For. Glob. Chang. 5, 1070372.

Bova, A.S., Mell, W.E., Hoffman, C.M., 2015. A comparison of level set and marker methods for the simulation of wildland fire front propagation. Int. J. Wildland Fire 25 (2), 229–241.

Bowman, D.M., Williamson, G.J., Abatzoglou, J.T., Kolden, C.A., Cochrane, M.A., Smith, A.M., 2017. Human exposure and sensitivity to globally extreme wildfire events. Nature Ecol. Evol. 1 (3), 0058.

Buccolieri, Riccardo, Santiago, Jose-Luis, Rivas, Esther, Sanchez, Beatriz, 2018. Review on urban tree modelling in CFD simulations: Aerodynamic, deposition and thermal effects. Urban Forestry & Urban Greening 31, 212–220.

Calkin, David E, O'Connor, Christopher D, Thompson, Matthew P, Stratton, Richard D, 2021. Strategic wildfire response decision support and the risk management assistance program. Forests 12 (10), 1407.

Churchill, D.J., Larson, A.J., Dahlgreen, M.C., Franklin, J.F., Hessburg, P.F., Lutz, J.A., 2013. Restoring forest resilience: from reference spatial patterns to silvicultural prescriptions and monitoring. Forest Ecol. Manag. 291, 442–457.

Doerr, S.H., Santín, C., 2016. Global trends in wildfire and its impacts: perceptions versus realities in a changing world. Philos. Trans. R. Soc. B 371, 20150345.

Drury, Stacy A, Rauscher, H Michael, Banwell, Erin M, Huang, ShihMing, Lavezzo, Tami L, 2016. The interagency fuels treatment decision support system: functionality for fuels treatment planning. Fire Ecol. 12, 103–123.

Ferrarese, Jena, Affleck, David, Seielstad, Carl, 2015. Conifer crown profile models from terrestrial laser scanning. Silva Fennica 49 (1), Finnish Society of Forest Science.

Fiedler, Carl E., Metlen, Kerry L., Dodson, Erich K., 2010. Restoration Treatment Effects on Stand Structure, Tree Growth, and Fire Hazard in a Ponderosa Pine/Douglas-Fir Forest in Montana. Forest Sci. 56 (1), 18–31.

Flannigan, M.D., Stocks, B.J., Wotton, B.M., 2000. Climate change and forest fires. Sci. Total Environ. 262 (3), 221–229.

Graham, R.T., McCaffrey, S., Jain, T.B., 2004. Science Basis for Changing Forest Structure to Modify Wildfire Behavior and Severity. (RMRS–GTR–120), USDA Forest Service, Rocky Mountain Research Station, Fort Collins, CO, p. 43.

Gray, Andrew N., Brandeis, Thomas J., Shaw, John D., McWilliams, William H., Miles, Patrick, 2012. Forest Inventory and Analysis Database of the United States of America (FIA). Biodiversity & Ecol. 225–231.

Halofsky, J.E., Peterson, D.L., Harvey, B.J., 2020. Changing wildfire, changing forests: the effects of climate change on fire regimes and vegetation in the Pacific Northwest, USA. Fire Ecol. 16 (1), 1–26.

Hessburg, P.F., Miller, C.L., Parks, S.A., Povak, N.A., Taylor, A.H., Higuera, P.E., Prichard, S.J., North, M.P., Collins, B.M., Hurteau, M.D., Larson, A.J., 2019. Climate, environment, and disturbance history govern resilience of western North American forests. Front. Ecol. Evol. 7, 239.

Hiers, J. Kevin, O'Brien, Joseph J., Varner, J. Morgan, Butler, Bret W., Dickinson, Matthew, Furman, James, Gallagher, Michael, Godwin, David, Goodrick, Scott L., Hood, Sharon M., Hudak, Andrew, Kobziar, Leda N., Linn, Rodman, Loudermilk, E. Louise, McCaffrey, Sarah, Robertson, Kevin, Rowell, Eric M., Skowronski, Nicholas, Watts, Adam C., Yedinak, Kara M., 2020. Prescribed fire science: the case for a refined research agenda. Fire Ecol. 16 (1), Publisher: Springer.

Hillman, S., Wallace, L., Reinke, K., Jones, S., 2021. A comparison between TLS and UAS LiDAR to represent eucalypt crown fuel characteristics. ISPRS J. Photogramm. Remote Sens. 181, 295–307.

Hoffman, C.M., Linn, R., Parsons, R., Sieg, C., Winterkamp, J., 2015. Modeling spatial and temporal dynamics of wind flow and potential fire behavior following a mountain pine beetle outbreak in a lodgepole pine forest. Agricult. Forest. Meterol. 204, 79–93.

Hoffman, C.M., Sieg, C.H., Linn, R.R., Mell, W., Parsons, R.A., Ziegler, J.P., Hiers, J.K., 2018. Advancing the science of wildland fire dynamics using process-based models. Fire 1 (2), 32.

Ingalsbee, T., 2017. Whither the paradigm shift? Large wildland fires and the wildfire paradox offer opportunities for a new paradigm of ecological fire management. Int. J. Wildland Fire 26 (7), 557–561.

Jenkins, Jennifer C., Chojnacky, David C., Heath, Linda S., Birdsey, Richard A., 2003. National scale biomass estimators for United States tree species. Forest Sci. 49, 12–35.

Kreider, Mark R., Higuera, Philip E., Parks, Sean A., Rice, William L., White, Nadia, Larson, Andrew J., 2024. Fire suppression makes wildfires more severe and accentuates impacts of climate change and fuel accumulation. Nature Commun. 15 (1), 2412, Publisher: Nature Publishing Group.

LANDFIRE, 2022. LANDFIRE: 40 Scott and Burgan Fire Behavior Fuel Models. U.S. Department of the Interior, Geological Survey, and U.S. Department of Agriculture, Available: 2023, August25.

Lannom, K.O., Tinkham, W.T., Smith, A.M., Abatzoglou, J., Newingham, B.A., Hall, T.E., Morgan, P., Strand, E.K., Paveglio, T.B., Anderson, J.W., Sparks, A.M., 2014. Defining extreme wildland fires using geospatial and ancillary metrics. Int. J. Wildland Fire 23 (3), 322–337.

Larson, A.J., Churchill, D., 2012. Tree spatial patterns in fire-frequent forests of western north america, including mechanisms of pattern formation and implications for designing fuel reduction and restoration treatments. Forest Ecol. Manag. 267, 74–92.

Linn, R.R., Goodrick, S.L., Brambilla, S., Brown, M.J., Middleton, R.S., O'Brien, J.J., Hiers, J.K., 2020. QUIC-fire: A fast-running simulation tool for prescribed fire planning. Environ. Model. Softw. 125, 104616.

Linn, R., Reisner, J., Colman, J.J., Winterkamp, J., 2002. Studying wildfire behavior using FIRETEC. Int. J. Wildland Fire 11 (4), 233–246.

Linn, R.R., Sieg, C.H., Hoffman, C.M., Winterkamp, J.L., McMillin, J.D., 2013. Modeling wind fields and fire propagation following bark beetle outbreaks in spatially-heterogeneous pinyon-juniper woodland fuel complexes. Agricult. Forest. Meterol. 173, 139–153.

Linn, Rodman, Winterkamp, Judith, Colman, Jonah J., Edminster, Carleton, Bailey, John D., 2005. Modeling interactions between fire and atmosphere in discrete element fuel beds. Int. J. Wildland Fire 14 (1), 37–48, Publisher: CSIRO PUBLISHING.

Lorensen, William E., Cline, Harvey E., 1987. Marching cubes: A high resolution 3D surface construction algorithm. ACM SIGGRAPH Comput. Graph. 21 (4), 163–169.

Loudermilk, E. Louise, O'Brien, Joseph J., Goodrick, Scott L., Linn, Rodman R., Skowronski, Nicholas S., Hiers, J. Kevin, 2022. Vegetation's influence on fire behavior goes beyond just being fuel. Fire Ecol. 18 (1), 9.

Loudermilk, E.L., Scheller, R.M., Weisberg, P.J., Kretchun, A., 2017. Bending the carbon curve: fire management for carbon resilience under climate change. Landsc. Ecol. 32, 1461–1472.

Marcozzi, Anthony A., Johnson, Jesse V., Parsons, Russell A., Flanary, Sarah J., Seielstad, Carl A., Downs, Jacob Z., 2023. Application of LiDAR derived fuel cells to wildfire modeling at laboratory scale. Fire 6 (10), 394, Number: 10 Publisher: Multidisciplinary Digital Publishing Institute.

Masson-Delmotte, V., Zhai, P., Pirani, A., Connors, S.L., Péan, C., Berger, S., Caud, N., Chen, Y., Goldfarb, L., Gomis, M.I., Huang, M., Leitzell, K., Lonnoy, E., Matthews, J.B.R., Maycock, T.K., Waterfield, T., Yelekçi, O., Yu, R., Zhou, B., 2021. Climate Change 2021: The Physical Science Basis. Cambridge University Press, Cambridge, United Kingdom and New York, NY, USA, pp. 3–32, Contribution of Working Group I to the Sixth Assessment Report of the Intergovernmental Panel on Climate Change,

McDanold, Jenna S., Linn, Rodman R., Jonko, Alex K., Atchley, Adam L., Goodrick, Scott L., Hiers, J. Kevin, Hoffman, Chad M., Loudermilk, E. Louise, O'Brien, Joseph J., Parsons, Russell A., Sieg, Carolyn H., Oliveto, Julia A., 2023. DUET - Distribution of Understory using Elliptical Transport: A mechanistic model of leaf litter and herbaceous spatial distribution based on tree canopy structure. Ecol. Model. 483, 110425.

McGrattan, Kevin, McDermott, Randall, Weinschenk, Craig, Forney, Glenn, 2013. Fire Dynamics Simulator Users Guide, sixth ed. Special Publication (NIST SP), National Institute of Standards and Technology, Gaithersburg, MD.

Mell, W., Jenkins, M.A., Gould, J., Cheney, P., 2007. A physics-based approach to modelling grassland fires. Int. J. Wildland Fire 16 (1), 1–22.

Molina, J.R., Ortega, M., Rodríguez y Silva, F., 2022. Scorch height and volume modeling in prescribed fires: Effects of canopy gaps in *Pinus pinaster* stands in Southern Europe. Forest Ecol. Manag. 506, 119979.

Moody, Matthew J., Gibbs, Jeremy A., Krueger, Steven, Mallia, Derek, Pardyjak, Eric R., Kochanski, Adam K., Bailey, Brian N., Stoll, Rob, Moody, Matthew J., Gibbs, Jeremy A., Krueger, Steven, Mallia, Derek, Pardyjak, Eric R., Kochanski, Adam K., Bailey, Brian N., Stoll, Rob, 2022. QES-Fire: a dynamically coupled fast-response wildfire model. Int. J. Wildland Fire 31 (3), 306–325, Publisher: CSIRO PUBLISHING.

Moran, C.J., Hoff, V., Parsons, R.A., Queen, L.P., Seielstad, C.A., 2022. Mapping fine-scale crown scorch in 3D with remotely piloted aircraft systems. Fire 5 (3), 59.

Mori, Shigeta, Hagihara, Akio, 1991. Crown profile of foliage area characterized with the Weibull distribution in a hinoki (*Chamaecyparis obtusa*) stand. Trees 5 (3), 149–152.

Murphy, Mary Carlton, Loudermilk, E. Louise, Pokswinski, Scott, Williams, Brett, Link, Emily, Lienesch, Laila, Douglas, Leta, Skowronski, Nicholas, Gallagher, Michael, Maxwell, Aaron, Snitker, Grant, Hawley, Christie, Wallace, Derek, Payne, Irenee, Yurkiewicz, Tim, Meador, Andrew J. Sánchez, Anderson, Chad, Jackson, J. Mark, Parsons, Russell, Floca, Melissa, Nealey, Isaac, Altintas, Ilkay, Hiers, J. Kevin, Wallace, Jon, 2024. Terrestrial 3D Laser Scanning for Ecosystem and Fire Effects Monitoring. http://dx.doi.org/10.1101/2024.04.09.587551, Pages: 2024.04.09.587551 Section: Confirmatory Results.

Noonan-Wright, Erin K, Opperman, Tonja S, Finney, Mark A, Zimmerman, G Thomas, Seli, Robert C, Elenz, Lisa M, Calkin, David E, Fiedler, John R, et al., 2011. Developing the US wildland fire decision support system. J. Combust. 2011.

OpenStreetMap contributors, 2017. Planet dump retrieved from https://planet.osm.org, https://www.openstreetmap.org.

Parsons, R.A., Linn, R.R., Pimont, F., Hoffman, C., Sauer, J., Winterkamp, J., Sieg, C.H., Jolly, W.M., 2017. Numerical investigation of aggregated fuel spatial pattern impacts on fire behavior. Land 6 (2), 43.

Parsons, R.A., Pimont, F., Wells, L., Cohn, G., Jolly, W.M., de Coligny, F., Rigolot, E., Dupuy, J.L., Mell, W., Linn, R.R., 2018. Modeling thinning effects on fire behavior with STANDFIRE. Ann. Forest Sci. 75 (1), 1–10.

Peeler, Jamie L, McCauley, Lisa, Metlen, Kerry L, Woolley, Travis, Davis, Kimberley T, Robles, Marcos D, Haugo, Ryan D, Riley, Karin L, Higuera, Philip E, Fargione, Joseph E, et al., 2023. Identifying opportunity hot spots for reducing the risk of wildfire-caused carbon loss in western US conifer forests. Environ. Res. Lett. 18 (9), 094040.

Pimont, F., Parsons, R., Rigolot, E., de Coligny, F., Dupuy, J.L., Dreyfus, P., Linn, R.R., 2016. Modeling fuels and fire effects in 3D: model description and applications. Environ. Model. Softw. 80, 225–244.

Purves, Drew W., Lichstein, Jeremy W., Pacala, Stephen W., 2007. Crown plasticity and competition for canopy space: A new spatially implicit model parameterized for 250 North American Tree Species. Plos One 2 (9), e870, Publisher: Public Library of Science.

QGIS Development Team, 2024. QGIS Geographic Information System. QGIS Association.

Radeloff, V.C., Helmers, D.P., Kramer, H.A., et al., 2018. Rapid growth of the U.S. wildland-urban interface raises wildfire risk. Proc. Natl. Acad. Sci. 115 (13), 3314–3319.

Reinhardt, Elizabeth, Crookston, Nicholas L., 2003. The Fire and Fuels Extension to the Forest Vegetation Simulator. In: Gen. Tech. Rep. RMRS-GTR-116, vol. 116, U.S. Department of Agriculture, Forest Service, Rocky Mountain Research Station., Ogden, UT, p. 209.

Riley, Karin L., Grenfell, Isaac C., Finney, Mark A., Wiener, Jason M., 2021. TreeMap, a tree-level model of conterminous US forests circa 2014 produced by imputation of FIA plot data. Sci. Data 8 (1), 11, Number: 1 Publisher: Nature Publishing Group.

Ritter, S.M., Hoffman, C.M., Battaglia, M.A., Linn, R., Mell, W.E., 2023. Vertical and horizontal crown fuel continuity influences group-scale ignition and fuel consumption. Fire 6 (8), 321.

Rocha, K.D., Silva, C.A., Cosenza, D.N., Mohan, M., Klauberg, C., Schlickmann, M.B., Xia, J., Leite, R.V., de Almeida, D.R.A., Atkins, J.W., Cardil, A., 2023. Crown-level structure and fuel load characterization from airborne and terrestrial laser scanning in a longleaf pine (Pinus palustris Mill.) forest ecosystem. Remote Sens. 15 (4), 1002.

Roten, Daniel, Wells, Lucas, Crawl, Daniel, Parsons, Russell A., Marcozzi, Anthony, Linn, Rodman R., Hiers, Kevin, Altintas, Ilkay, 2023. TrueTrees: A scalable workflow for the integration of airborne LiDAR scanning data into fuel models for prescribed fire simulations. In: 2023 IEEE 19th International Conference on E-Science. E-Science, pp. 1–10, ISSN: 2325-3703.

Rothermel, R.C., 1972. A Mathematical Model for Predicting Fire Spread in Wildland Fuels, vol. 115, Intermountain Forest & Range Experiment Station, Forest Service, US Department of Agriculture.

Sánchez-López, Nuria, Hudak, Andrew T., Boschetti, Luigi, Silva, Carlos A., Robertson, Kevin, Loudermilk, E Louise, Bright, Benjamin C., Callaham, Mac A., Taylor, Melanie K., 2023. A spatially explicit model of tree leaf litter accumulation in fire maintained longleaf pine forests of the southeastern US. Ecol. Model. 481, 110369.

Scott, Joe H., Burgan, Robert E., 2005. Standard fire behavior fuel models: A comprehensive set for use with Rothermel's surface fire spread model. In: USDA Forest Service - General Technical Report RMRS-GTR, (no. 153 RMRS-GTR), pp. 1–76.

Stephens, Scott L., Collins, Brandon M., Biber, Eric, Fulé, Peter Z., 2016. U.S. federal fire and forest policy: emphasizing resilience in dry forests. Ecosphere 7 (11), e01584, _eprint: https://onlinelibrary.wiley.com/doi/pdf/10.1002/ecs2.1584.

Turco, M., Abatzoglou, J.T., Herrera, S., Zhuang, Y., Jerez, S., Lucas, D.D., AghaKouchak, A., Cvijanovic, I., 2023. Anthropogenic climate change impacts exacerbate summer forest fires in California. Proc. Natl. Acad. Sci. 120 (25), e2213815120.

Turco, M., Rosa-Cánovas, J.J., Bedia, J., Jerez, S., Montávez, J.P., Llasat, M.C., Provenzale, A., 2018. Exacerbated fires in mediterranean europe due to anthropogenic warming projected with non-stationary climate-fire models. Nature Commun. 9 (1), 3821.

Vakili, Emma, Hoffman, Chad M., Keane, Robert E., Tinkham, Wade T., Dickinson, Yvette, 2016. Spatial variability of surface fuels in treated and untreated ponderosa pine forests of the southern Rocky Mountains. Int. J. Wildland Fire 25 (11), 1156–1168, Publisher: CSIRO PUBLISHING.

Vorster, Anthony G., Evangelista, Paul H., Stovall, Atticus E.L., Ex, Seth, 2020. Variability and uncertainty in forest biomass estimates from the tree to landscape scale: the role of allometric equations. Carbon Balance Manage. 15 (1), 8.

Westfall, James A., Coulston, John W., Gray, Andrew N., Shaw, John D., Radtke, Philip J., Walker, David M., Weiskittel, Aaron R., MacFarlane, David W., Affleck, David L.R., Zhao, Dehai, Temesgen, Hailemariam, Poudel, Krishna P., Frank, Jereme M., Prisley, Stephen P., Wang, Yingfang, Meador, Andrew J. Sánchez, Auty, David, Domke, Grant M., 2023. A national-scale tree volume, biomass, and carbon modeling system for the United States. In: Gen. Tech. Rep. WO-104, vol. 104, U.S. Department of Agriculture, Forest Service, Washington, DC.

Wilson, Barry T., Knight, Joseph F., McRoberts, Ronald E., 2018. Harmonic regression of Landsat time series for modeling attributes from national forest inventory data. ISPRS J. Photogramm. Remote Sens. 137, 29–46.

Yedinak, Kara M., Strand, Eva K., Hiers, J. Kevin, Varner, J. Morgan, 2018. Embracing complexity to advance the science of wildland fire behavior. Fire 1 (2), 1–8, Publisher: MDPI AG.

Young, J.D., Evans, A.M., Iniguez, J.M., Thode, A., Meyer, M.D., Hedwall, S.J., McCaffrey, S., Shin, P., Huang, C.H., 2020. Effects of policy change on wildland fire management strategies: evidence for a paradigm shift in the western US? Int. J. Wildland Fire 29 (10), 857–877.

Ziegler, J.P., Hoffman, C.M., Collins, B.M., Long, J.W., Dagley, C.M., Mell, W., 2020. Simulated fire behavior and fine-scale forest structure following conifer removal in aspen-conifer forests in the Lake Tahoe Basin, USA. Fire 3 (3), 51.